Chapter 5

Signal Analysis

5.1 Denoising fiber optic sensor signal

We first perform wavelet-based denoising on fiber optic sensor signals. Examine the fiber optic signal data (see Appendix B). Across all measurements, FB1 has the most significant spikes at time 0, where the trigger was set, so we first select the data set FB1 (012) as an example. Using Daubechies-8 (db8) wavelet, and performed a 4-level wavelet decomposition. Fig 24 shows the decomposed signals at each level.

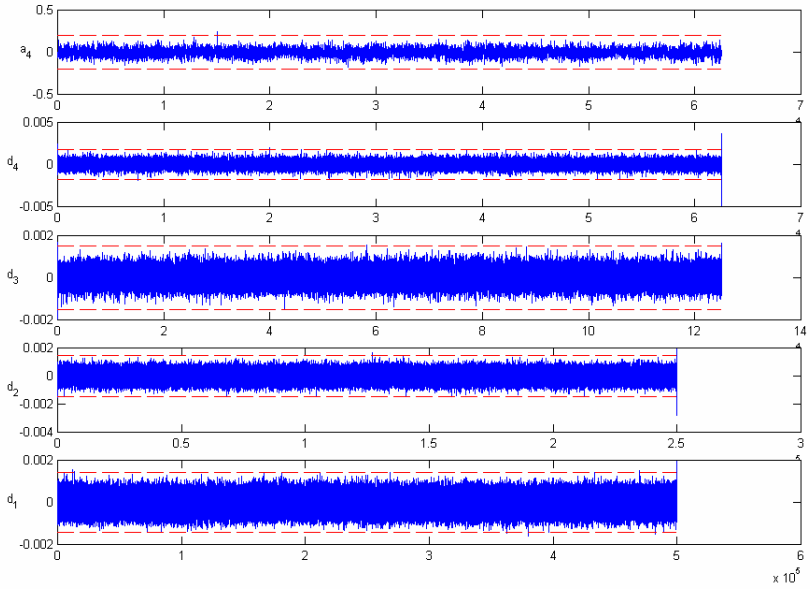

Fig 24. FB1 (012) 4-level wavelet decompositions using 'db8' as mother wavelet. 'a_4': the 4th level approximated signal. 'd_4': the 4th level detailed. 'd_3': the 3rd level detailed signal. 'd_2': the 2nd level detailed signal. 'd_1': the 1st level detailed signal. The dashed lines are the threshold limits at each signal.

As stated before, the noise in the original signal is also spanned in the decomposed signals. The second step to denoise the signals is to set the appropriate threshold, which, in this case, we select 4.5 times of the standard deviation of the wavelet-decomposed signal at each level. The dashed lines in Fig 24 indicate the upper and lower threshold limit for each decomposed signal. We then applied hard thresholding method to remove the noises in the signals. The denoised signal at each level is shown in Fig 25.

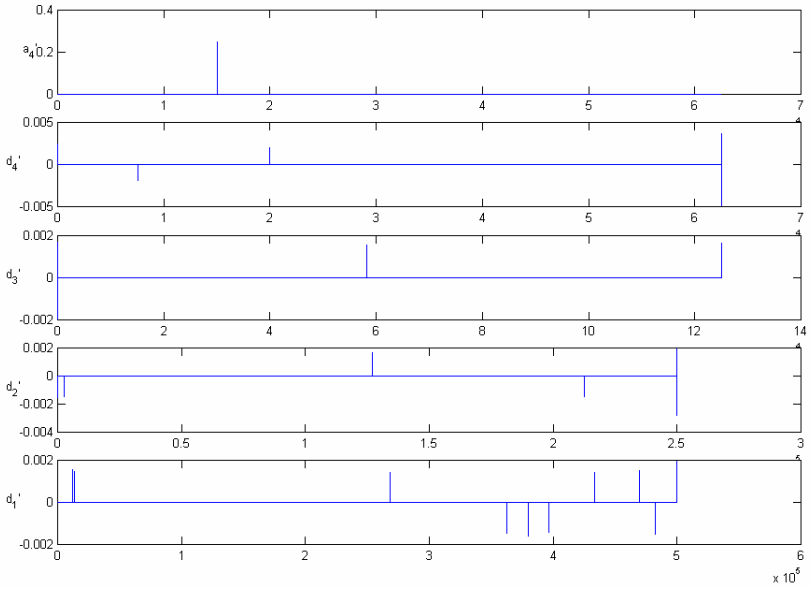

Fig 25. The approximated and detailed signal after hard thresholding of FB1 (012)

We could notice that only some spikes whose amplitudes are greater than the threshold limit are left. By performing an inverse wavelet transform on these thresholded-transformed signals, we could obtain an estimation of the original uncontaminated signal (Fig 26).

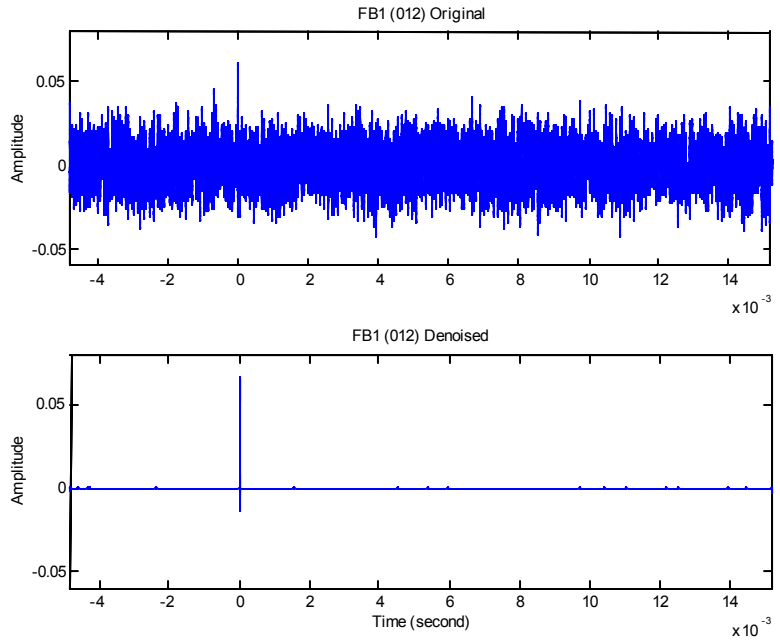

Fig 26. Original signal and denoised signal of FB1 (012).

Let's go back and examine why we select 'db8' wavelets but not others. As mentioned in 4.3, the selection of the mother wavelet could be based on several criteria – manual observation, correlation between original signal and denoised signal or cumulative energy relation over some interval of where PD signal occurs. We choose the later two criteria to compare how different mother wavelets would affect the correlation coefficients and the cumulative energy distribution.

If we zoom in the region around time 0 in Fig 26, where the most dominant PD spike occurs, shown in Fig 27, we could see that not only will the spike be capture by wavelet denoising procedure but also the denoised signal is not a single mother wavelet but linear combination of the mother wavelet. To find the relation between the original signal and the denoised signal about the most dominant spike, we calculate the correlation coefficient (Fig 28) between two signals by (21) and the cumulative energy distribution (Fig 30) by (22) around time 0. For other FB1 signals, we repeat the denoising procedure as mentioned and the calculation of the relation of two signals by applying different mother wavelet to the signals. The results are shown in Fig 31 to Fig 45.

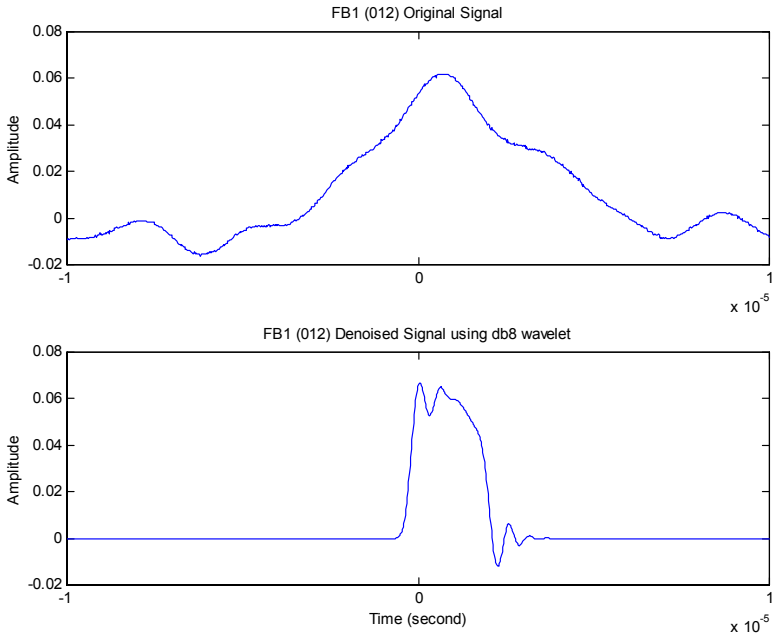

Fig 27. Zoom in around time 0 of FB1 (012) original vs. denoised signal using db8 wavelet

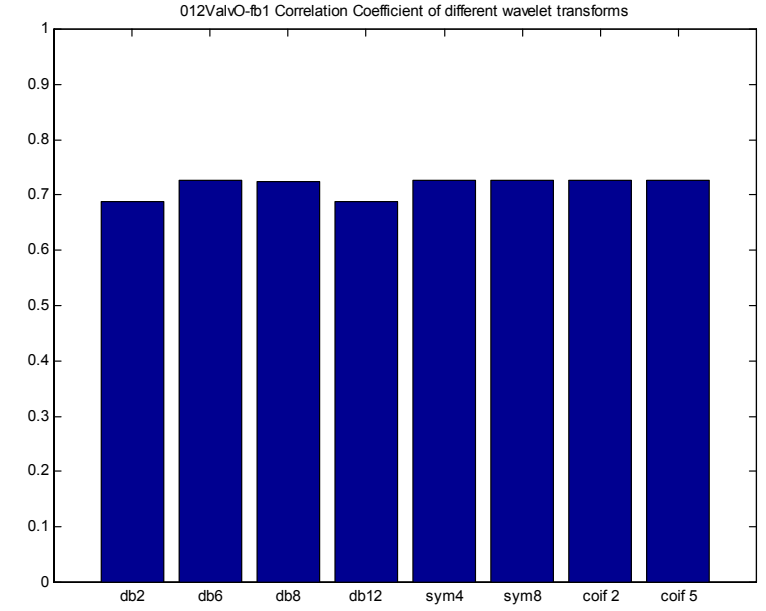

Fig 28. FB1 (012) Correlation coefficient of the denoised signal using different mother wavelets and the original signal between -10μ second and 10μ second interval. 'db2' = Daubechies 2. 'db6' = Daubechies 6. 'db8' = Daubechies 8. 'db12' = Daubechies 12. 'sym4' = Symlets 4. 'sym8' = Symlets 8. 'coif2' = Coiflets 2. 'coif5' = Coiflets 5.

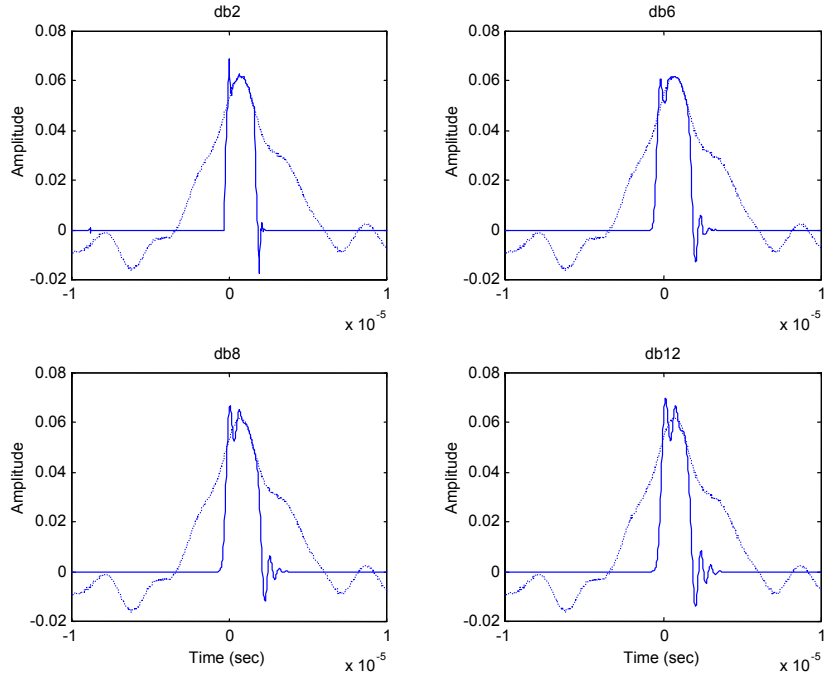

(a)

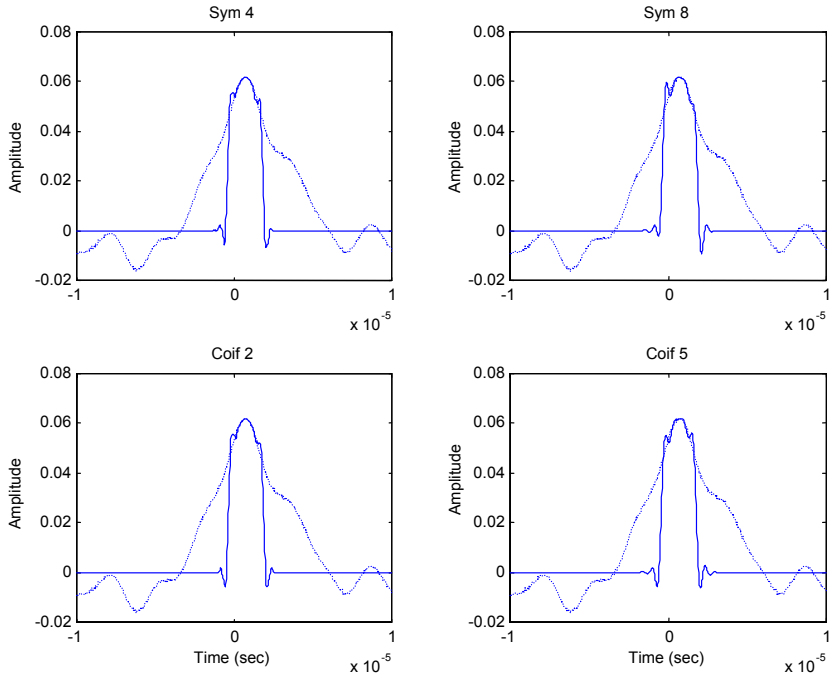

(b)

Fig 29 (a), (b). FB1 (012) Denoised signals using different wavelets between -10μ second and 10μ second interval. Solid line: denoised signal. Dashed line: original signal.

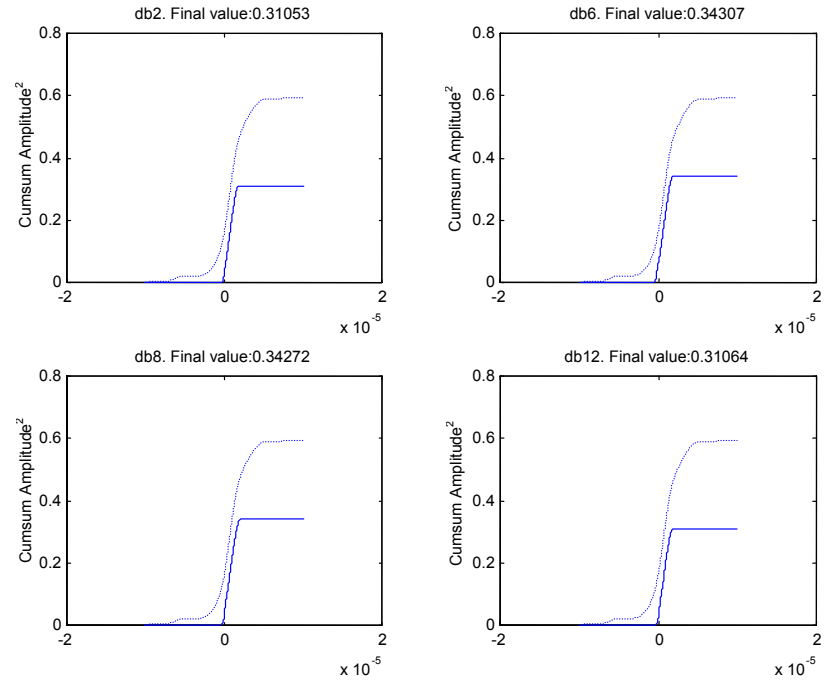

(a)

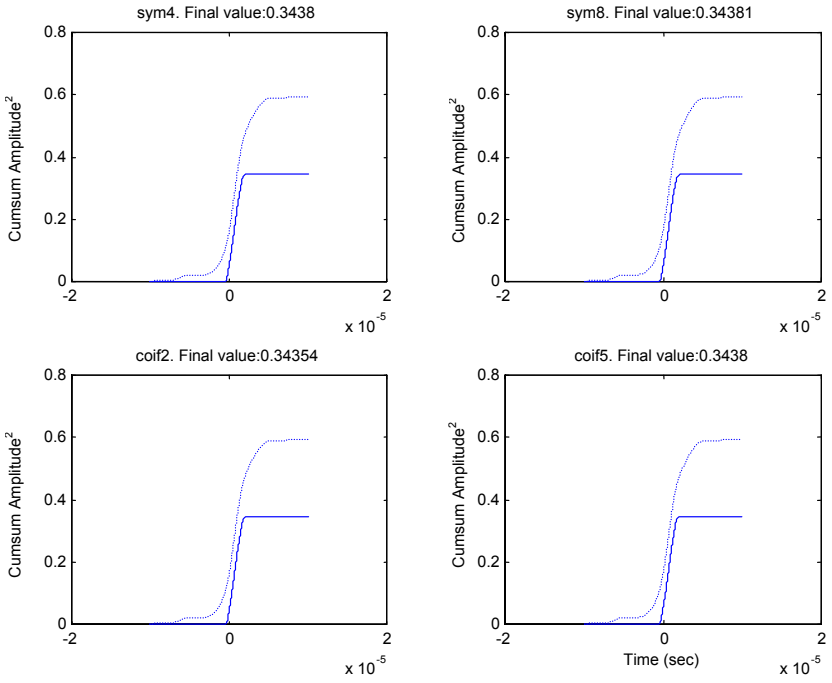

(b)

Fig 30 (a), (b). FB1 (012) Cumulative energy of denoised signals using different wavelets between -10μ second and 10μ second interval. Solid line: denoised signal. Dashed line: original signal.

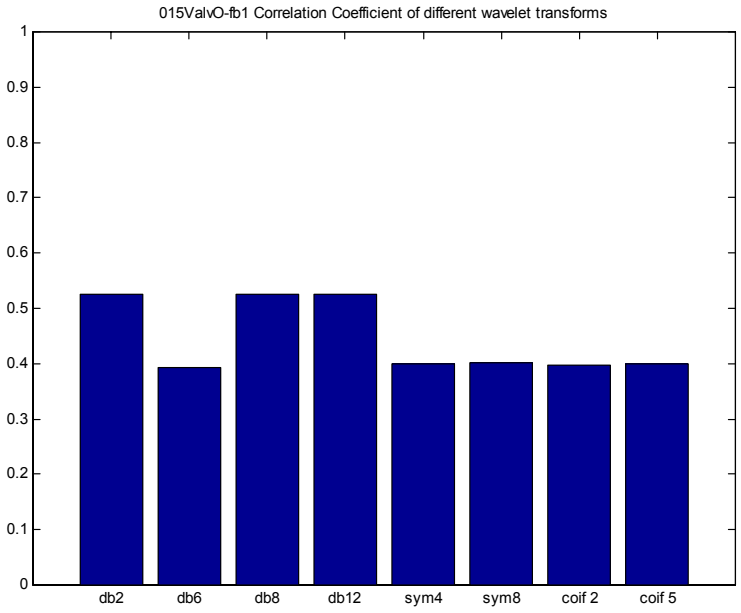

Fig 31. FB1 (015) Correlation coefficient of the denoised signal using different mother wavelets and the original signal between -10μ second and 10μ second interval.

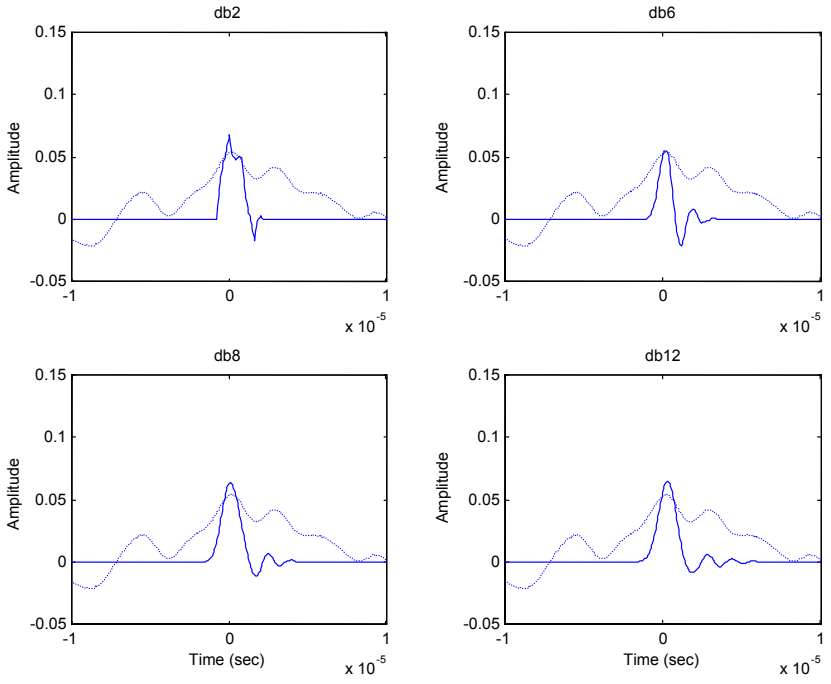

(a)

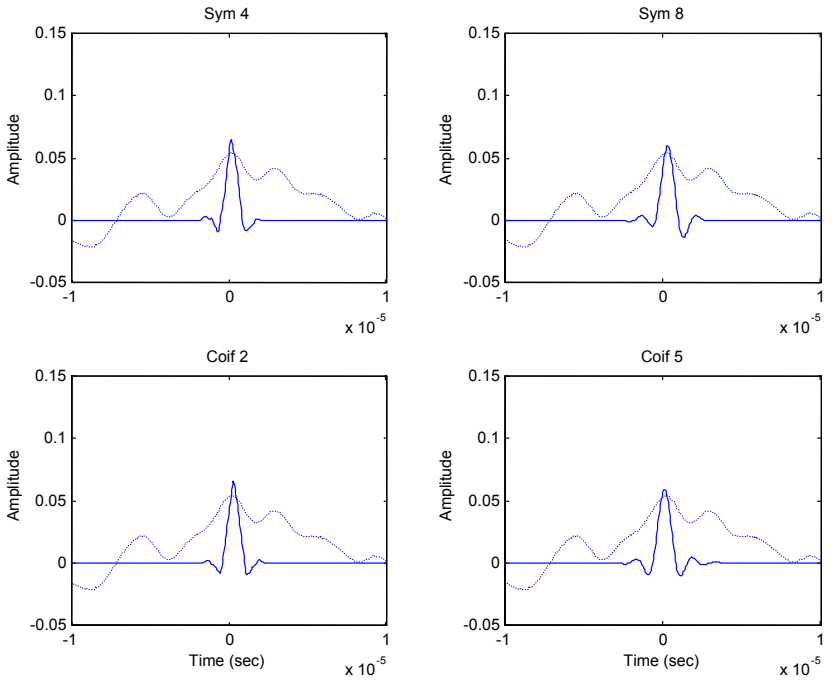

(b)

Fig 32 (a), (b). FB1 (015) Denoised signals using different wavelets between -10μ second and 10μ second interval. Solid line: denoised signal. Dashed line: original signal.

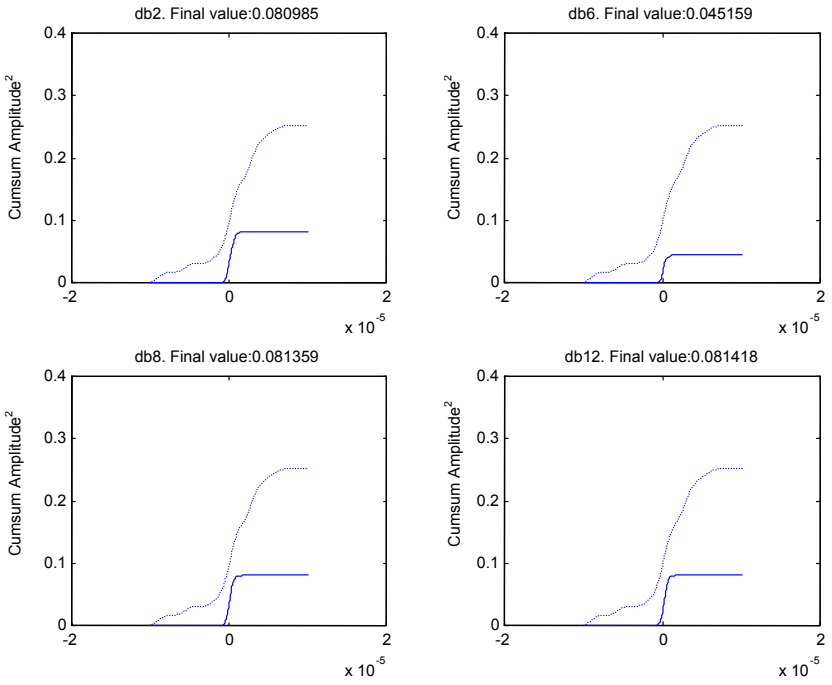

(a)

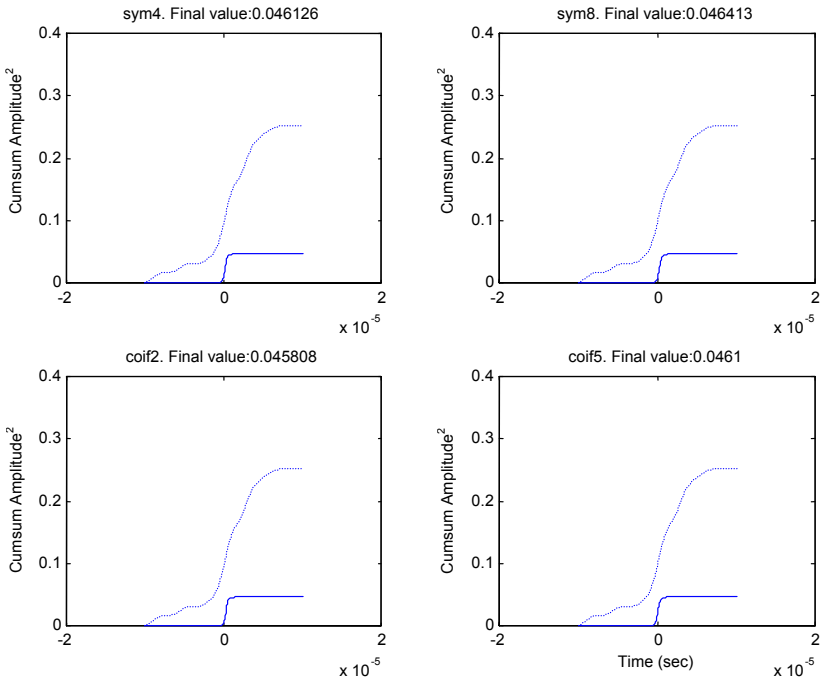

(b)

Fig 33 (a), (b). FB1 (015) Cumulative energy distribution of denoised signals using different wavelets between -10μ second and 10μ second interval. Solid line: denoised signal. Dashed line: original signal.

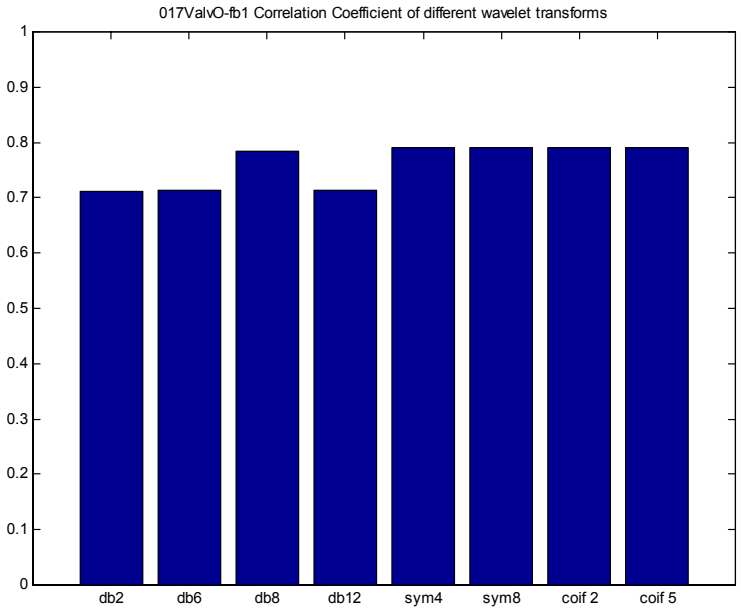

Fig 34. FB1 (017) Correlation coefficient of the denoised signal using different mother wavelets and the original signal between -10μ second and 10μ second interval.

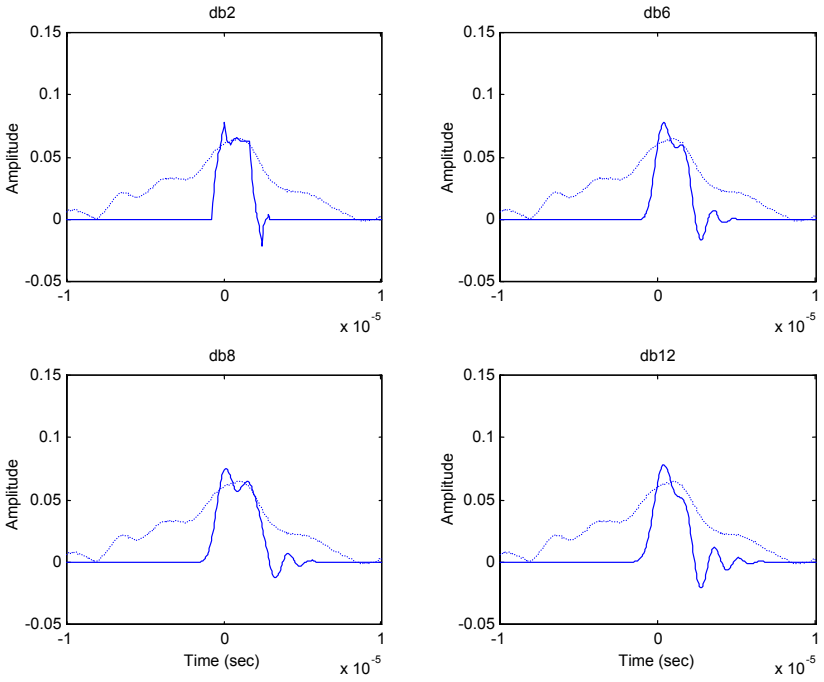

(a)

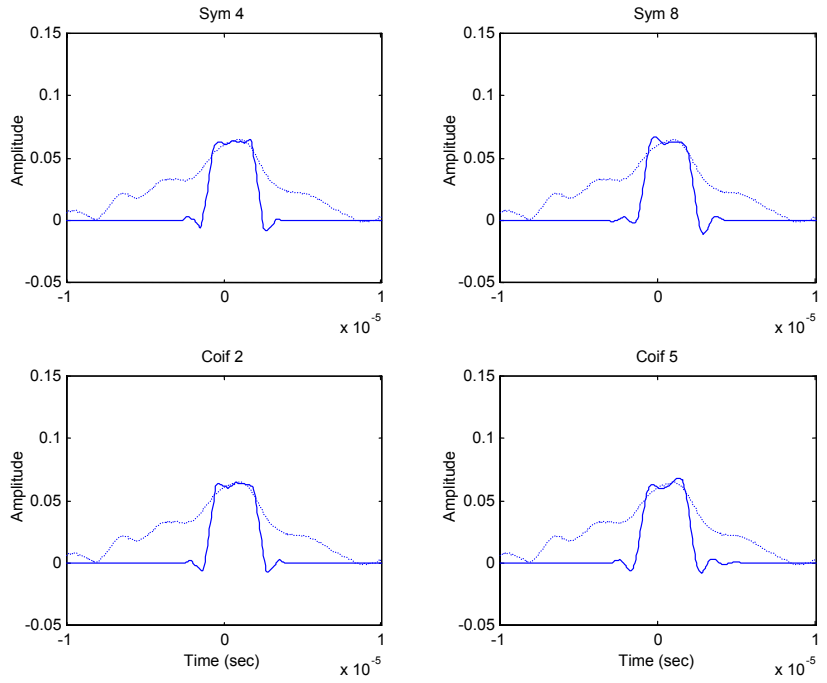

(b)

Fig 35 (a), (b). FB1 (017) denoised signals using different wavelets between -10μ second and 10μ second interval. Solid line: denoised signal. Dashed line: original signal.

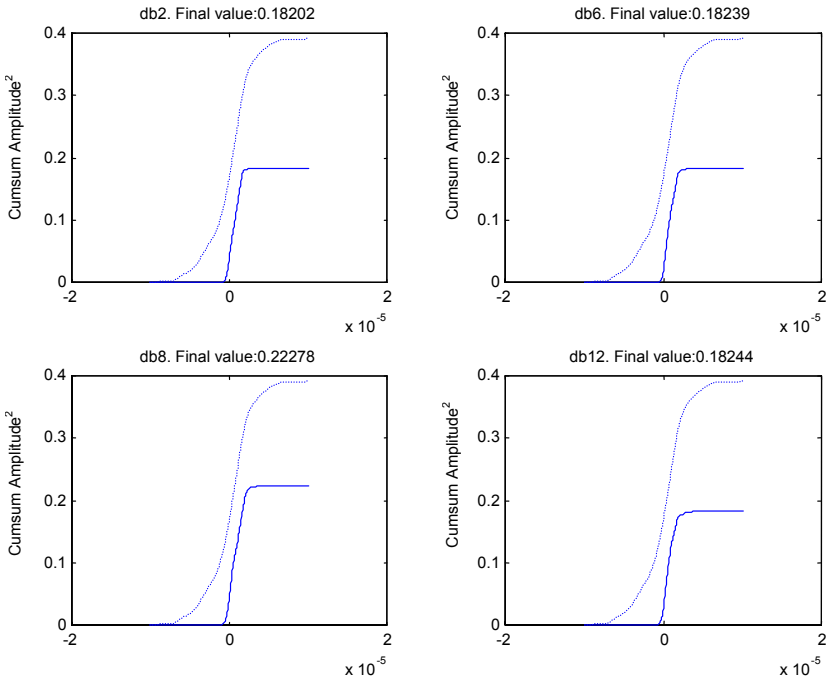

(a)

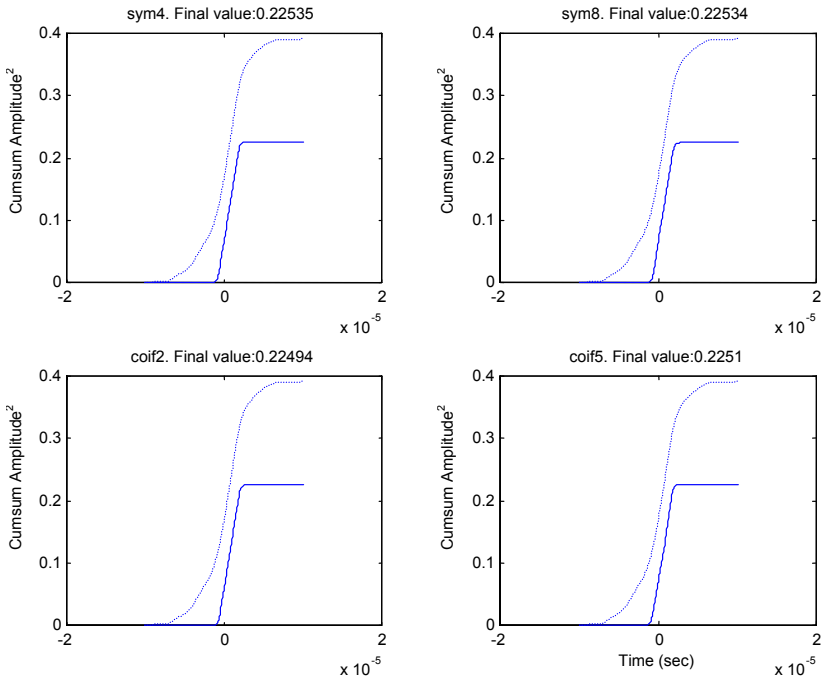

(b)

Fig 36 (a), (b). FB1 (017) Cumulative energy distribution of denoised signals using different wavelets between -10μ second and 10μ second interval. Solid line: denoised signal. Dashed line: original signal.

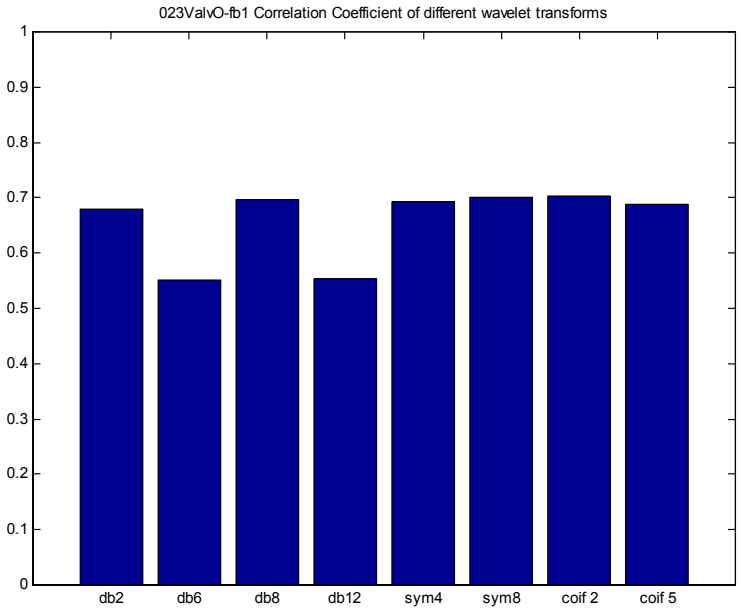

Fig 37. FB1 (023) Correlation coefficient of the denoised signal using different mother wavelets and the original signal between -10μ second and 10μ second interval.

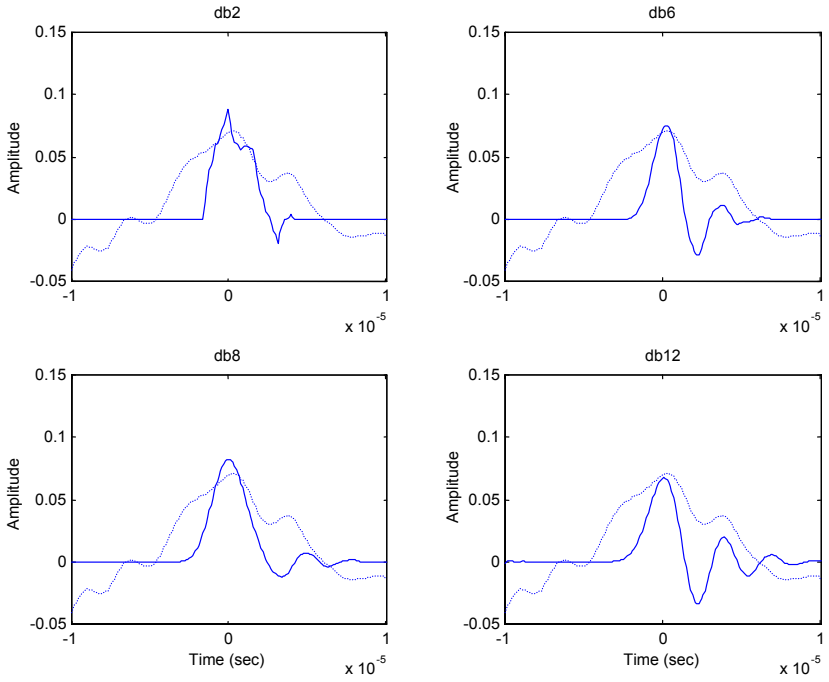

(a)

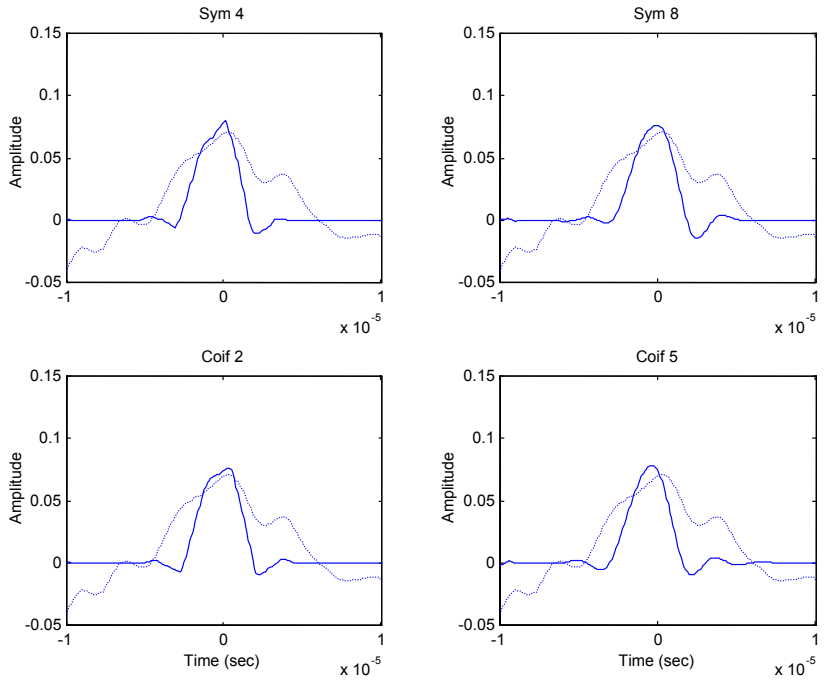

(b)

Fig 38 (a), (b). FB1 (023) denoised signals using different wavelets between -10μ second and 10μ second interval. Solid line: denoised signal. Dashed line: original signal.

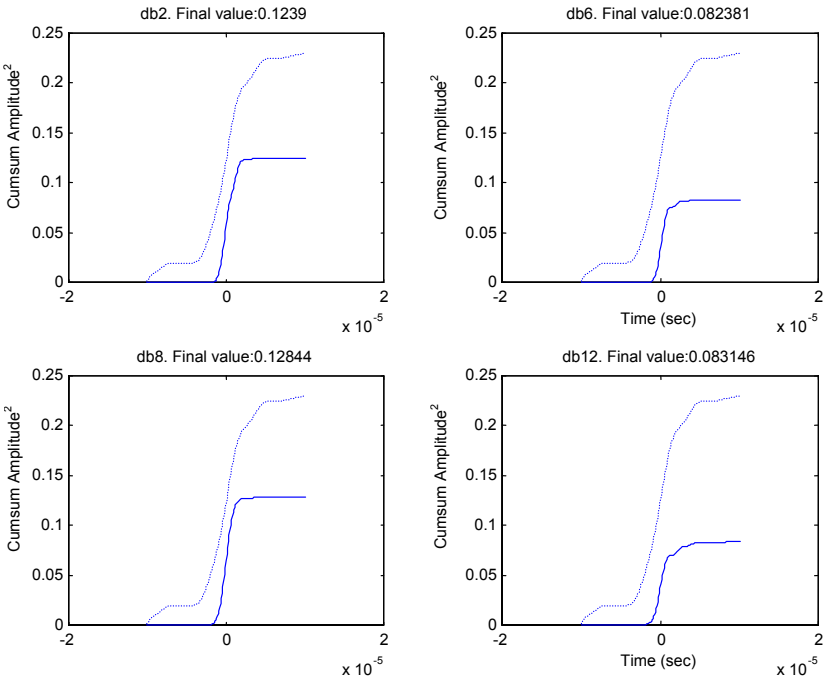

(a)

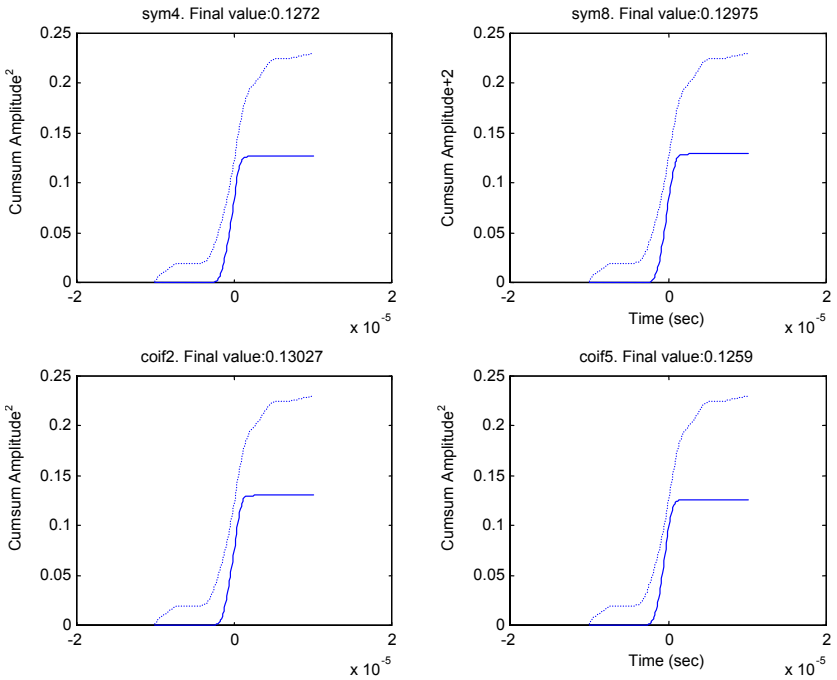

(b)

Fig 39 (a), (b). FB1 (023) Cumulative energy distribution of denoised signals using different wavelets between -10μ second and 10μ second interval. Solid line: denoised signal. Dashed line: original signal.

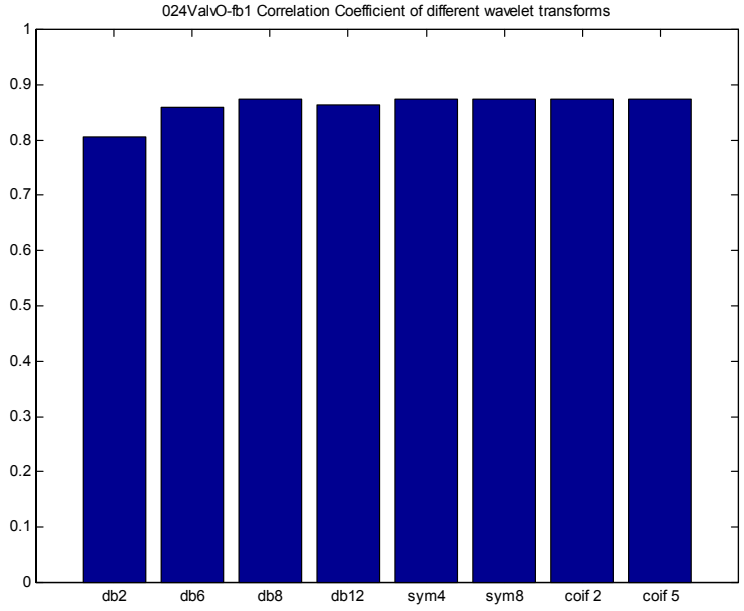

Fig 40. FB1 (024) Correlation coefficient of the denoised signal using different mother wavelets and the original signal between -10μ second and 10μ second interval.

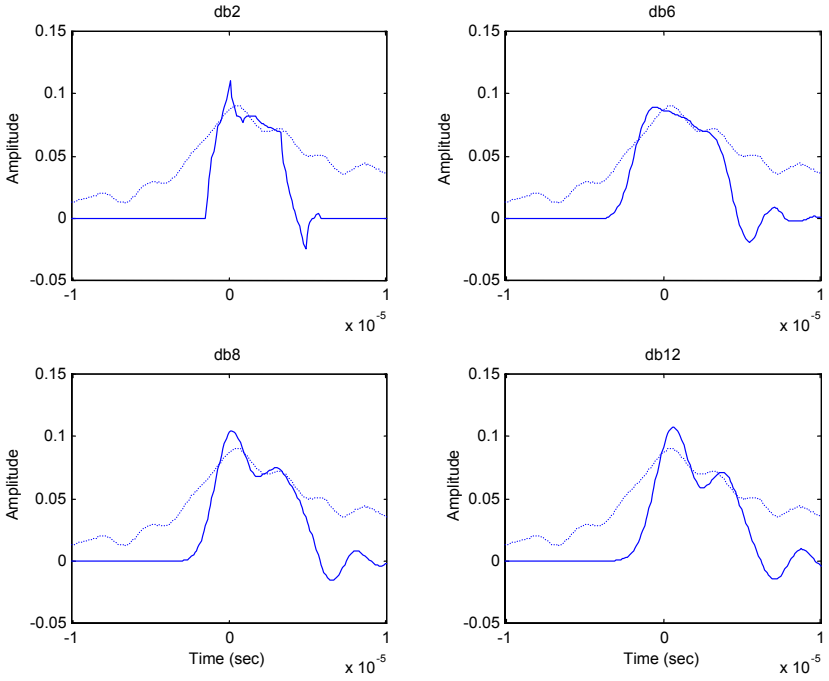

(a)

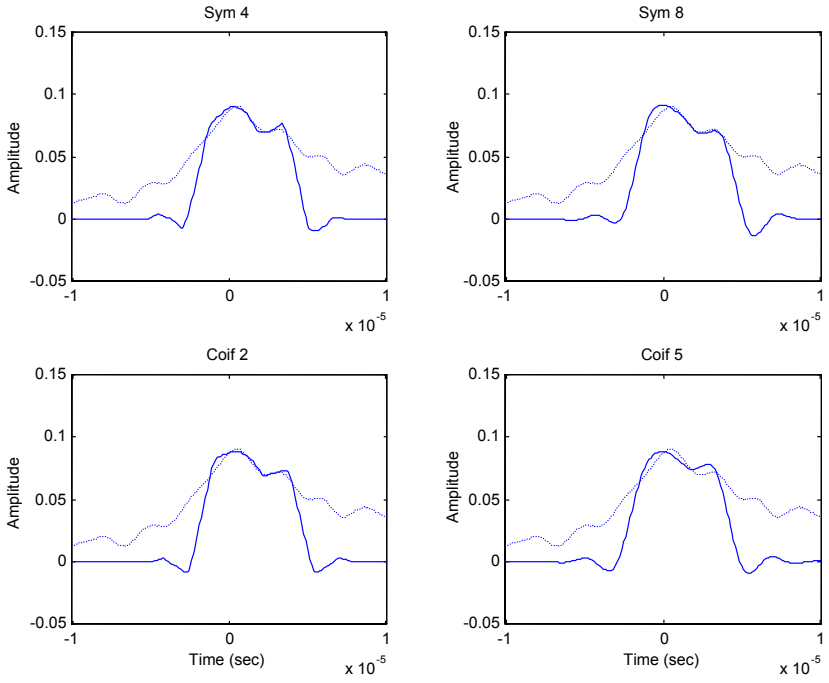

(b)

Fig 41 (a), (b). FB1 (024) denoised signals using different wavelets between -10μ second and 10μ second interval. Solid line: denoised signal. Dashed line: original signal.

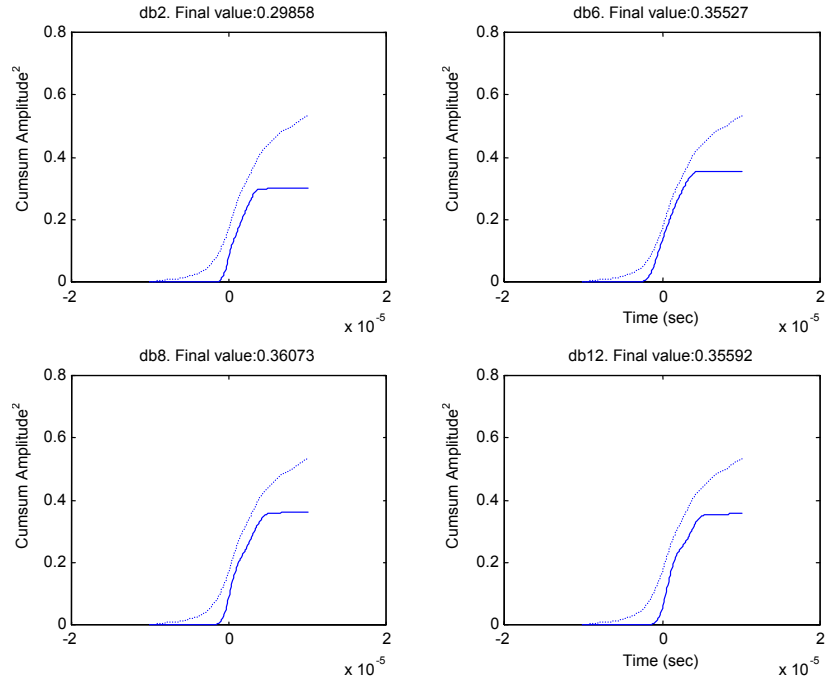

(a)

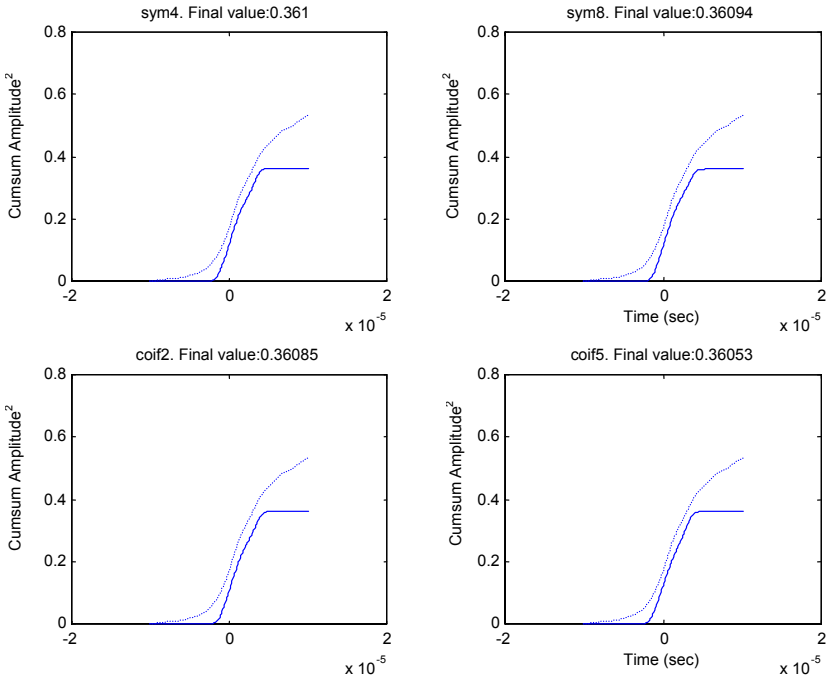

(b)

Fig 42 (a), (b). FB1 (024) Cumulative energy distribution of denoised signals using different wavelets between -10μ second and 10μ second interval. Solid line: denoised signal. Dashed line: original signal.

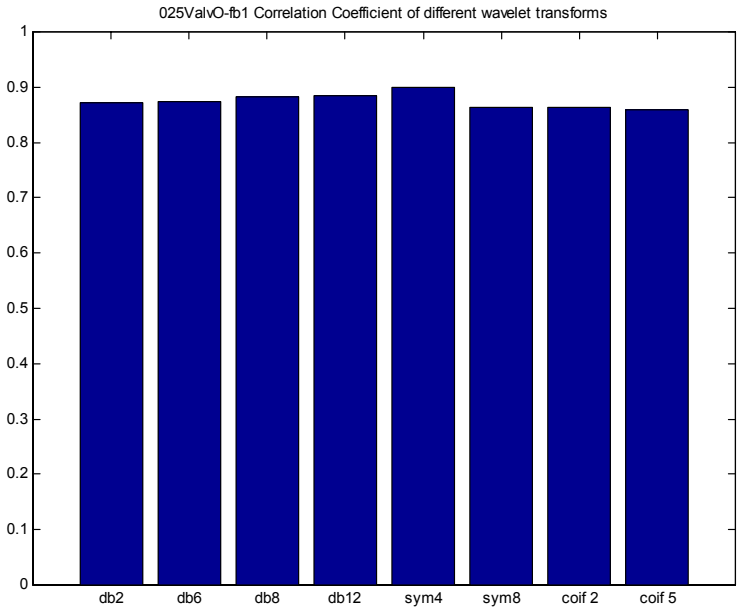

Fig 43. FB1 (025) Correlation coefficient of the denoised signal using different mother wavelets and the original signal between -10μ second and 20μ second interval.

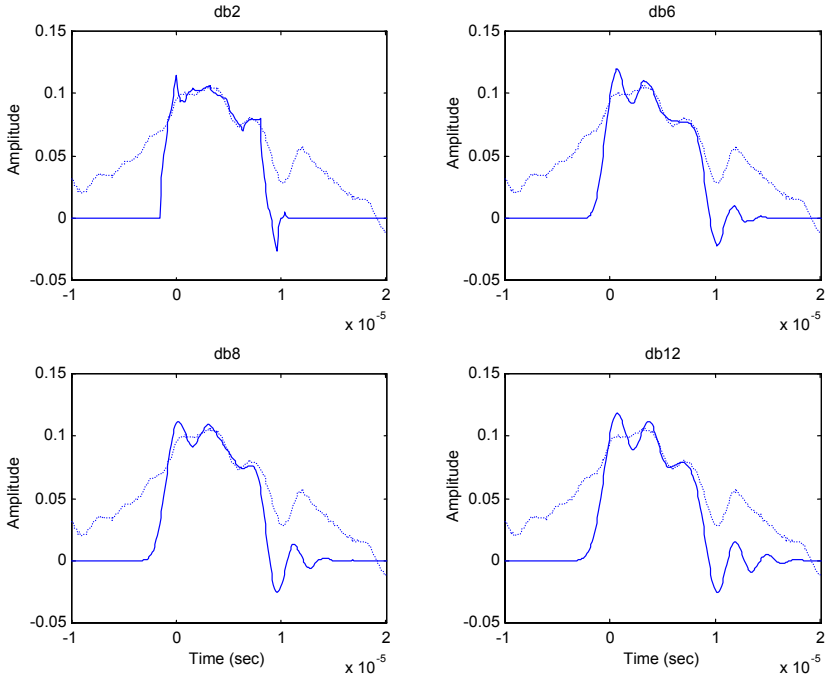

(a)

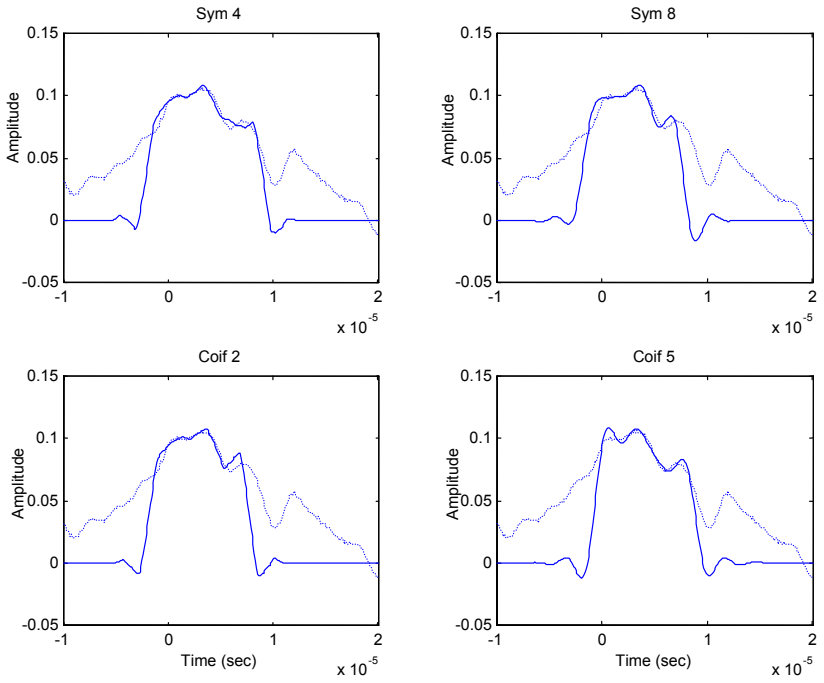

(b)

Fig 44 (a), (b). FB1 (025) denoised signals using different wavelets between -10μ second and 20μ second interval. Solid line: denoised signal. Dashed line: original signal.

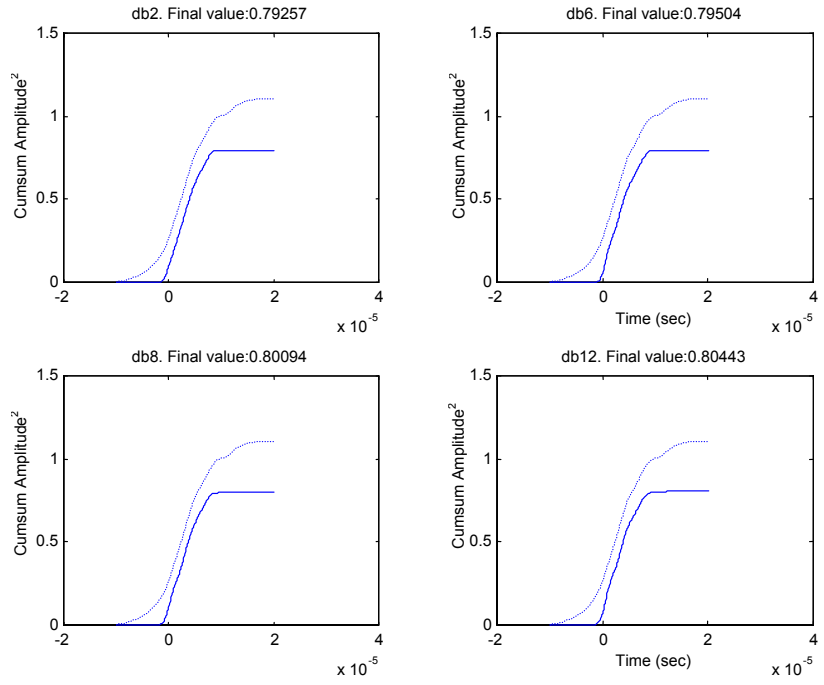

(a)

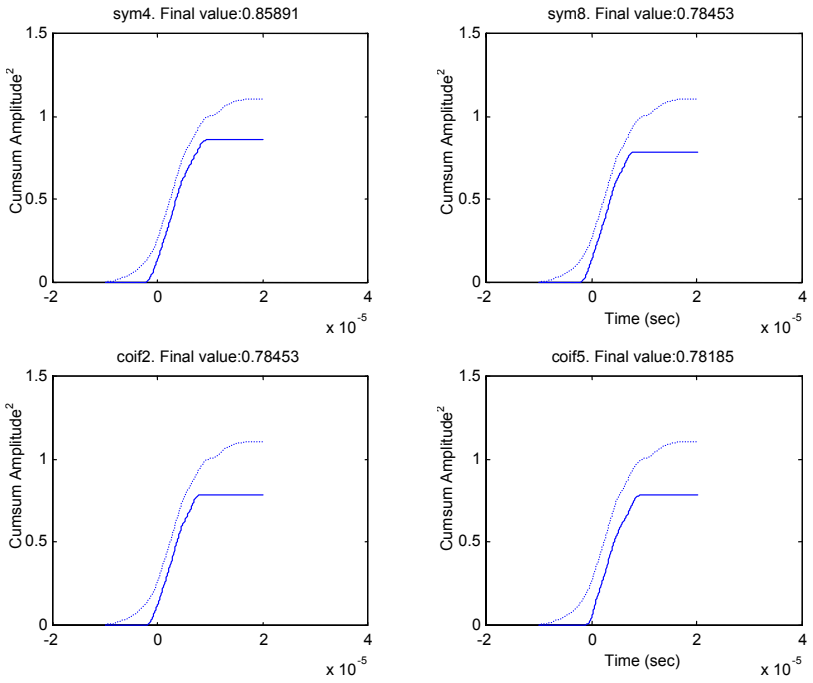

(b)

Fig 45 (a), (b). FB1 (025) Cumulative energy distribution of denoised signals using different wavelets between –10μ second and 20μ second interval. Solid line: denoised signal. Dashed line: original signal.

From Fig 28 to Fig 45, we could observe that the spikes measured by fiber optic sensor is like an impulse waveform, the Daubechies wavelets would capture it more likely than Symlets or Coiflets, since Symlets and Coiflets have the symmetric waveform shape about its maximum peak value. Among all the Daubechies wavelets, 'db8' tends to have higher correlation coefficient of the denoised signal and original signal; and higher cumulative energy around where the PD spike occurs. Therefore, we select 'db8' as the mother wavelet for the wavelet decomposition for fiber optic sensor signal.

5.2 Denoising PZT sensor signal

Denoising the PZT measurement data follows the same procedure as stated in the previous section. The differences are that the threshold limits in this case are tuned manually, since the signal-to-noise ratio in this case is higher and Gaussian noise is not

dominant anymore in the decomposed signals so we could not use solely the rule of multiplication of standard deviation of the signal to determine the threshold limit. Secondly, the level needed in the wavelet decomposition is higher.

Take PZTBI (012) as an example. We perform the wavelet-based denoising procedure. Here we use Daubechies 2, 'db2', as the mother wavelet and perform 12-level wavelet transform. Fig 46 shows the decomposed approximated signal at the 12th level and detailed signals at level 12 and the following levels.

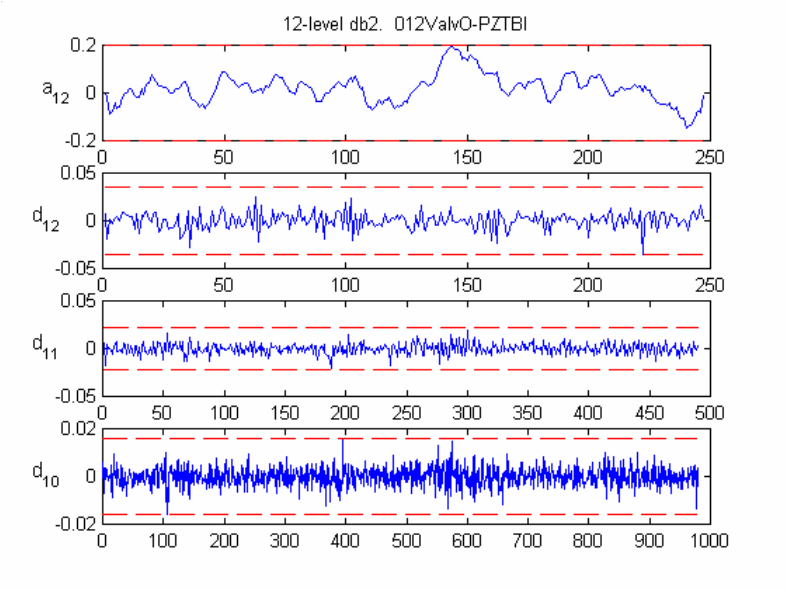

(a)

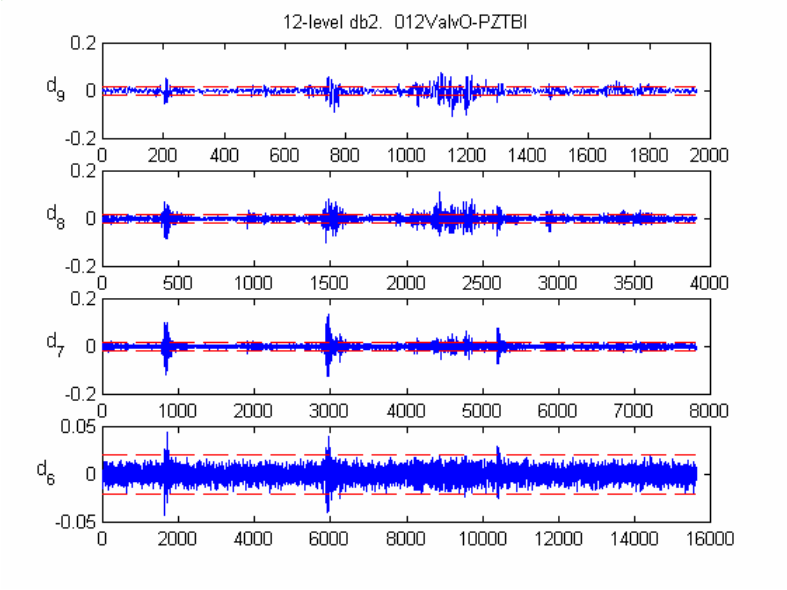

(b)

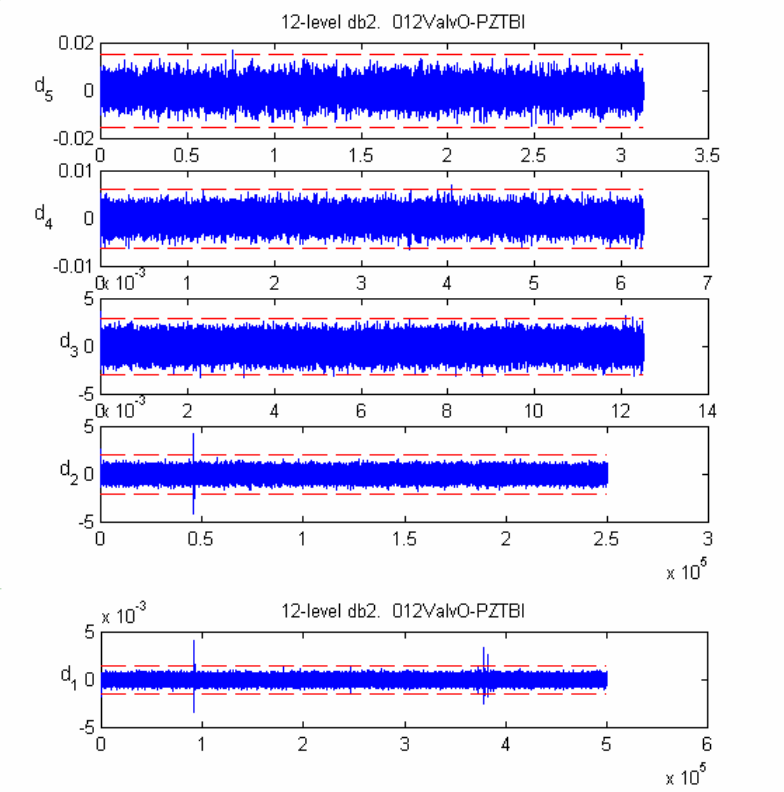

(c)

Fig 46. PZTBI (012) 12-level wavelet decompositions using 'db2' as mother wavelet. (a) a_{12}, d_{12}, d_{11}, d_{10}; (b) d_9, d_8, d_7, d_6; (c) d_5, d_4, d_3, d_2, d_1. 'a' and 'd' are the approximated and detailed signal, respectively. The number in subscript represents the level of wavelet transform. Dashed line indicates the threshold limit we choose for each decomposed signal.

From Fig 46, we could observe that there are three different signatures of signals. Here a12 resembles the DC variation of the measured signal. d10, d11 and d12 contain mainly noises. d6 to d9 signals show some similarities between each other; in addition, they resemble to the major spike group shown in the original signal (Fig 47). d5-d1 signals are composed of mainly Gaussian noise. Therefore, the threshold limits for these three different characteristic signals have to be chosen independently. We select to remove the DC variation, a12. For Gaussian noise like signal, we select 4.5 times of signal standard deviation as the threshold limit. For those mid-level detailed wavelet decomposed signals, we set the threshold limit such that the white noise spanned across the signal could be removed.

Applying inverse wavelet transform of the thresholded transformed signals, we could estimate the original uncontaminated signal shown in Fig 47.

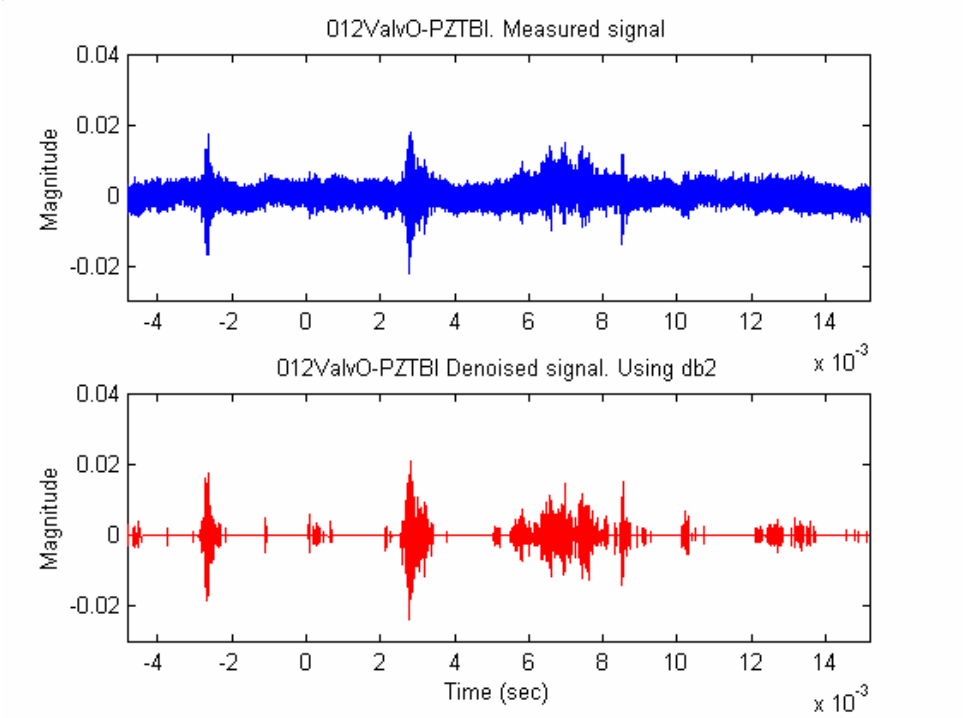

Fig 47. PZTBI (012) measured signal and denoised signal using wavelet transfrom

Examining how different 'mother wavelets' affect the correlation coefficient between the original signal and denoised signal; and the cumulative energy distribution for PZT measured signals. We found that no matter which 'mother wavelet', e.g. Daubechies, Symlets, or Coiflets, the metrics to determine the similarity between two signals come out to be very close. Therefore, we select the mother wavelet for these PZT measured signal based on manual inspection and 'db2' seems to best fit the measured signals.

Other PZTBI measured signals and denoised signals can be found in **Appendix C**.

5.3 PZT measured signal statistics

From the PZT measured signals inside bottom valve (PZTBI) as shown in Fig 48, we can observe that some distinct burst groups appear across the measured signal. To better characterize these burst groups, some statistical metrics are analyzed including:

- Burst duration (second)
- Average and standard deviation of the PD burst group

- Maximum zero-to-peak amplitude

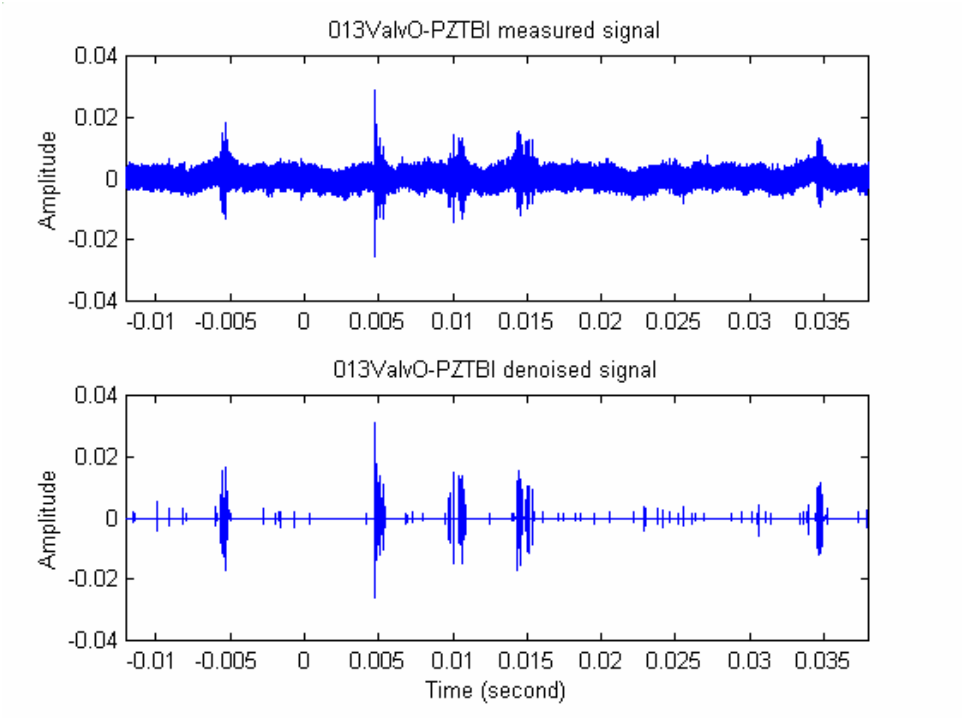

Fig 48. PZTBI (013) measured signal and denoised signal

We look at the major burst group in terms of the maximum peak magnitude, where in this case it is around 0.005 second. Fig 49 shows the zoomed measured signal and denoised signal in the interval of 0.0047 and 0.0055 second.

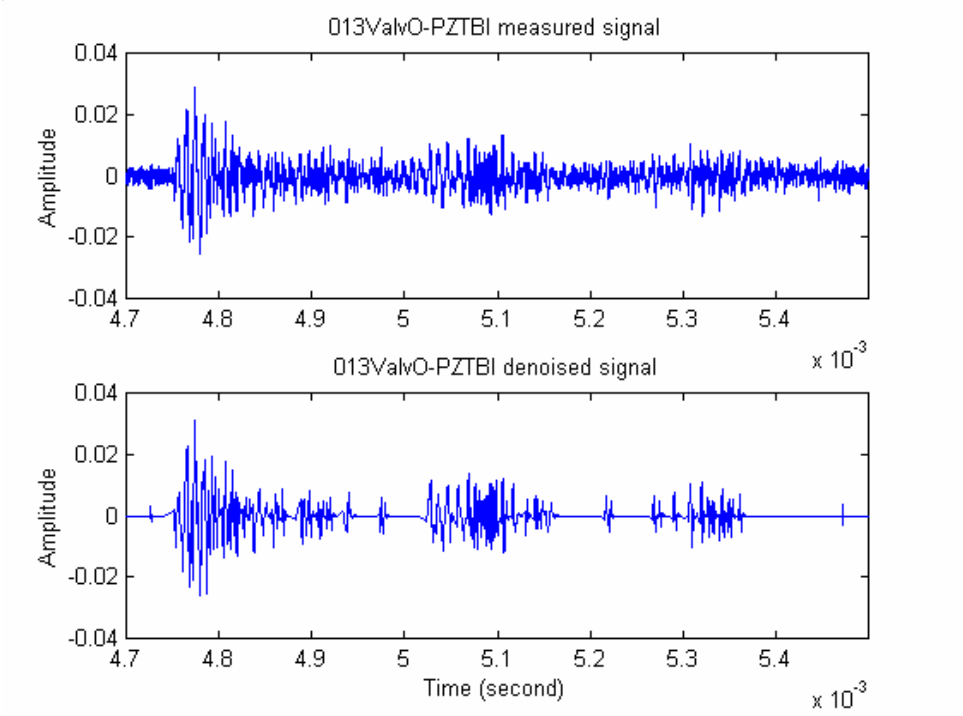

Fig 49. PZTBI (013) measured signal and denoised signal zoomed between 0.0047 and 0.0055 second

It is shown that the burst group contains 2 parts: the rapid rising part (up to the maximum amplitude) and the slowly decaying part. The wavelet-based denoising procedure demonstrated in section 5.2 can eliminate the DC component. In addition, for maximum Gaussian noise removal, the hard-thresholding with the case-by-case tuned threshold limits is applied to all sub-band detailed signals. The duration of the PD burst group can be estimated from the denoised signal, since the noises are removed so we are able to clearly identify at what time the burst initiates. Moreover, the mean and standard variation of the major burst group can be calculated. Some statistical results are shown in Table 2 and

Table 3 for measured signal and denoised signal, respectively.

Table 2. PZTBI measured signal statistical results

Measured signals				
Test #	Time interval of the major PD burst group (ms)	Major PD burst group amplitude average	Major PD burst group variance	Max. zero-to-peak voltage (mv) and occurring time (ms)

012	2.765 – 2.925	0.00051	0.0062	21.95 (2.78)
013	4.733 – 4.96	-0.00027	0.0066	28.68 (4.77)
016	-0.0452 – 0.2613	0.003	0.0049	18.51 (30.88)
017	0.3641 – 0.6843	-0.00013	0.0048	18.67 (0.438)
023	13.097 – 13.497	0.0026	0.0146	46.49 (13.198)
024	13.442 – 14.1613	0.0098	0.0195	86.18 (13.727)

(Note that for measured signal, the maximum zero-to-peak amplitude for the data set 016 is the only one that does not fall in the interval of major PD burst group.)

Table 3. PZTBI denoised signal statistical results

Denoised signals				
Test #	Time interval of the major PD burst group (ms)	Major PD burst group amplitude average	Major PD burst group variance	Max. zero-to-peak voltage (mv) and occurring time (ms)
012	2.765 – 2.925	~0	0.0052	22.19 (-2.66)
013	4.733 – 4.96	~0	0.0061	31.14 (4.77)
016	-0.0452 – 0.2613	~0	0.0043	20.74 (30.88)
017	0.3641 – 0.6843	~0	0.0043	22.29 (0.4377)
023	13.097 – 13.497	-0.00001	0.0111	47.62 (53.3)
024	13.442 – 14.1613	-0.000001	0.0192	85.07 (13.73)

From the measurements and statistical calculation, we found the following characteristics of the PZT measured signal:

- The duration of the major PD burst group is estimated between 0.2 to 0.4 msec.
- No consistency of the zero-to-peak amplitude is found between tests. The zero-to-peak amplitudes vary from 18.51 mV to 86.18mV.
- The means of the major PD burst group are about zero in measured and denoised signal. Variances of the major PD burst group stay with the same level for the similar zero-to-peak amplitudes.
- Randomness of peak amplitude, and time of duration.

5.4 Signal frequency analysis

5.4.1 Fiber optic sensor signal

As mentioned in the previous section, the nature of the PD signal is like an impulse signal above some noises. Without performing Fourier analysis to obtain a precise frequency spectrum, we could estimate the frequency of the PD signal manually from the graphs.

We first zoom in around time 0 neighborhood, where the PD signal occurs. From the graph, we can then estimate the time-width of the spike from both the top part of the spike and from the extension of the top part of the spike to zero crossing. Fig 50 shows an example of FB1 (012). If this spike curve were to be replaced by a sinusoid, the period of the sinusoid would be 2 times of the estimated time-width; therefore, we can calculate the estimated frequency of the spike. Other examples (FB1(017), FB1(024)) could be found in Fig 51 and Fig 52.

The estimated frequencies from these examples fall in the range of 70kHz to 250kHz.

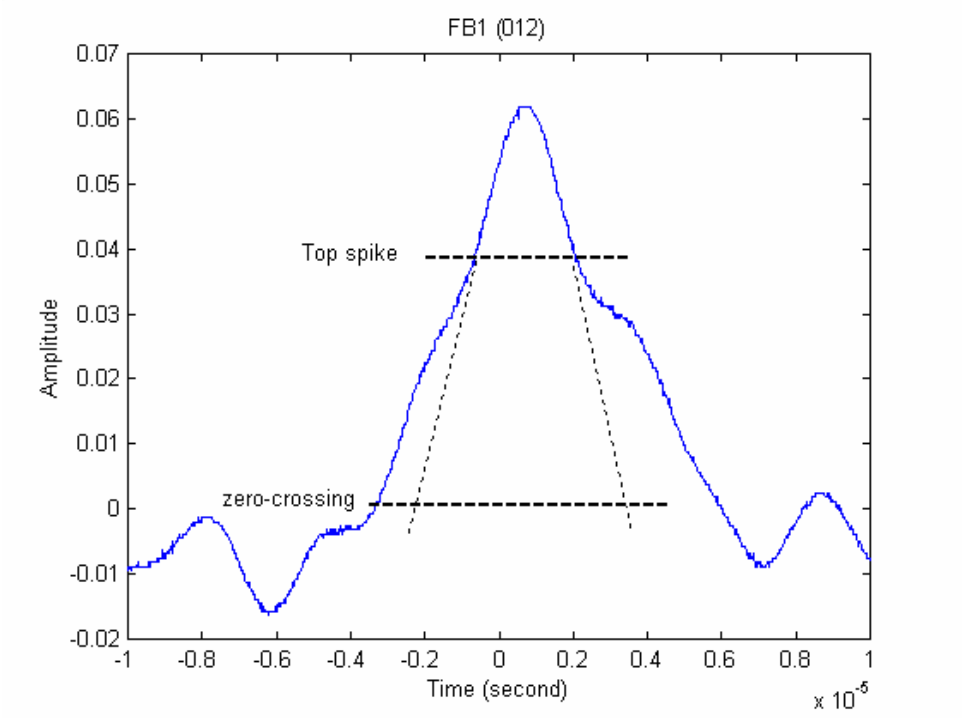

Fig 50. FB1 (012) estimation of PD spike frequency

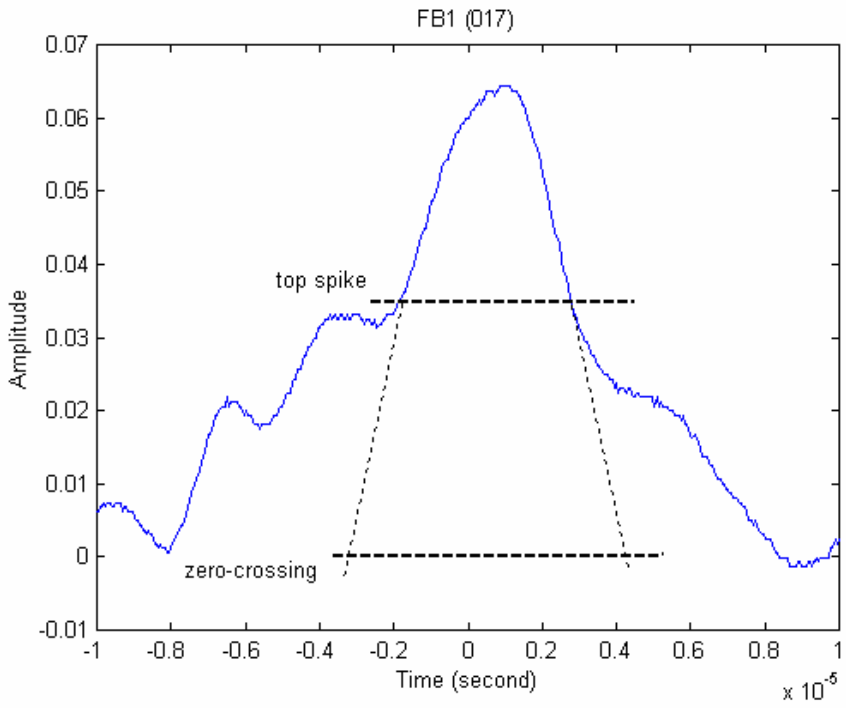

Fig 51. FB1 (017) estimation of PD spike frequency

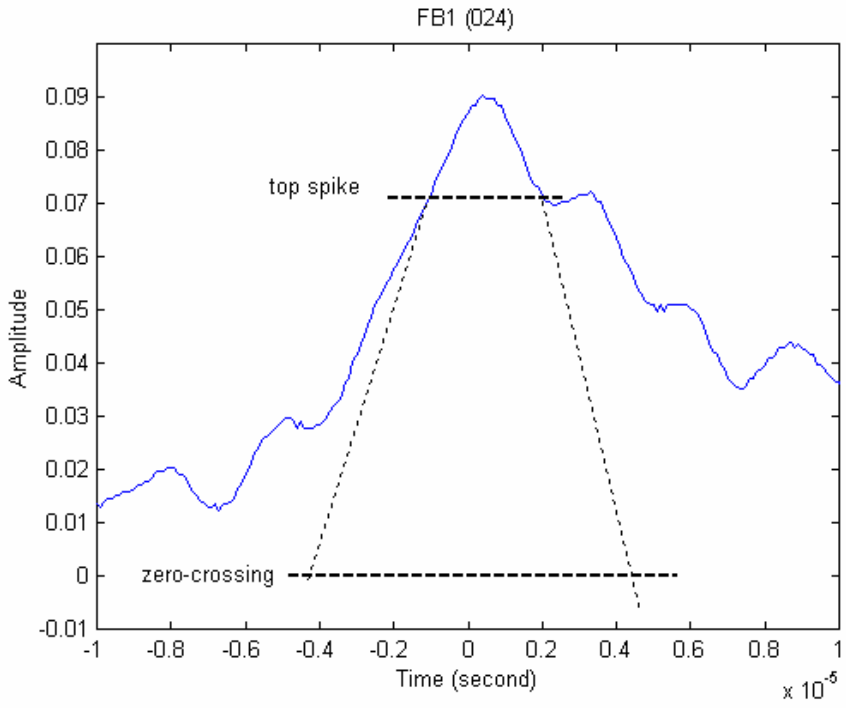

Fig 52. FB1 (024) estimation of PD spike frequency

5.4.2 PZT signal

For PZT measured signal, the frequency content can be obtained by discrete Fourier transform (DFT). We apply FT to the neighborhood of the major PD burst group. A typical measurement (PZTBI (013)) of time domain and frequency spectrum are shown as following:

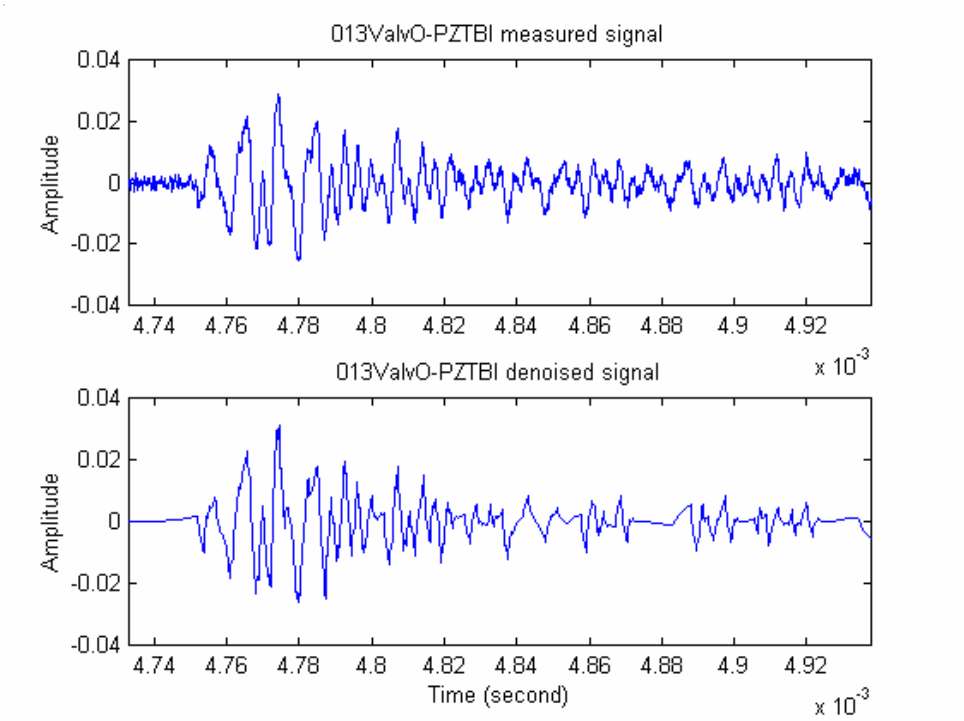

Fig 53. PZTBI (013) zoomed signal in the region of 4.73ms and 4.94ms. Top: measured signal. Bottom: Denoised signal

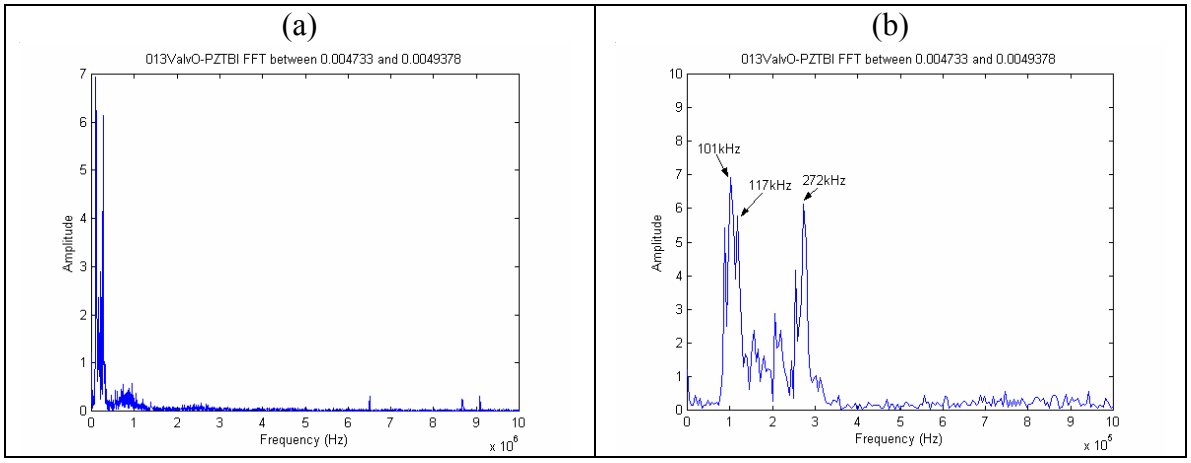

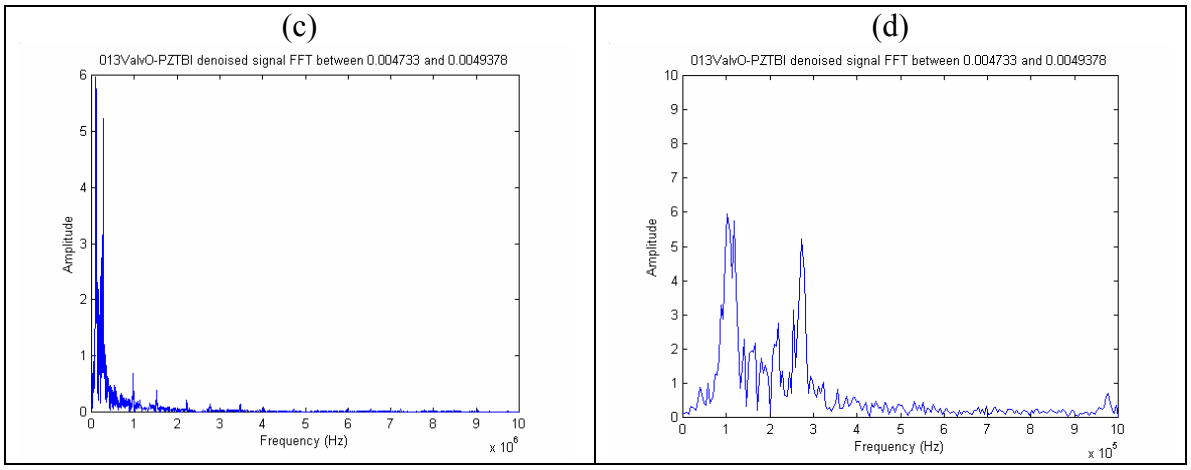

Fig 54. (a) DFT of measured signal (DC-10 MHz), (b) DFT of measured signal (DC-1MHz), (c) DFT of denoised signal (DC-10MHz), (d) DFT of denoised signal (DC-1MHz)

As it is shown, most of the energy is concentrated in 80kHz to 300kHz. Two groups of spikes around 100kHz and 250kHz appear in this data set and other measurements as shown in Appendix C.

It is shown that some noises related to the magnetization of the core winding could be present in the measurement. In [17], the author stated two types of noises due to magnetization: Barkhansen noise (BN) and Magnetomechanical Acoustic Emission (MAE). The Barkhansen noise is due to the sudden rotation of the magnetic dipole in the magnetic materials and it has the characteristics of the impulse signal appearing at the reflection point of magnetization current [17]. MAE noise is caused by the discontinuity movement of the magnetic dipole in the material therefore some stress impulse will be released. It is believed that the frequency of BN is concentrated below 20kHz whereas MAE is concentrated between 30kHz and 65kHz. From our measurement, we do not observe any major spike at these frequencies, so it is unlikely that our measurement is interfered by these two noises.

5.5 Signal occurrence phase analysis

In addition to the PD measurement from the sensors, we also recorded a reference transformer voltage sinusoid waveform simultaneously to study where PD occurrence in

a cycle of a sinusoid. Fig 55 illustrates how we define the quadrant of the PD occurrence with reference to a sinusoid waveform.

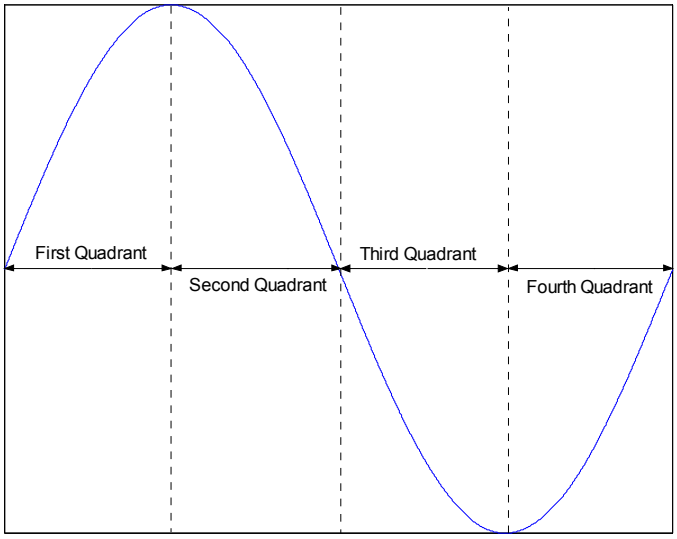

Fig 55. Quadrant definition based on sinusoid waveform

From some measurements (024-045), see Appendix D, assuming PD signal is the largest spike among all other spikes from the fiber optical sensor bottom 1 (FB1) measured signals, we can observe that PD signal was captured at time=0, due to the setting of the magnitude trigger. By manual inspection, we identified the PD signal occurrence phase in reference to a phase A sinusoid of the transformer voltage (the measured sinusoid leads phase A by 90°) as following:

Test Number	PD occurrence degree (direct reading from measurement by manual inspection)	PD occurrence degree (with the correction of -90°)
Valve Shut		
D027	n/a	n/a
D029	~50°	~320°
D030	~=90°	~=0°
D031	~130°	~40°
D032	~125°	~35°
D033	~100°	~10°

Valve Open		
D035	n/a	n/a
D036	~300°	~210°
D037	~225°	~135°
D038	~260°	~170°
D039	~250°	~160°
D040	~100°	~10°
D041	~250°	~160°
D042	~300°	~210°
D043	~230°	~140°
D044	~265°	~175°
D045	~250°	~160°
D024	~40°	~310°
D025	~45°	~315°
D026	~225°	~135°

Table 4. PD occurrence degree in reference to measured sinusoids.

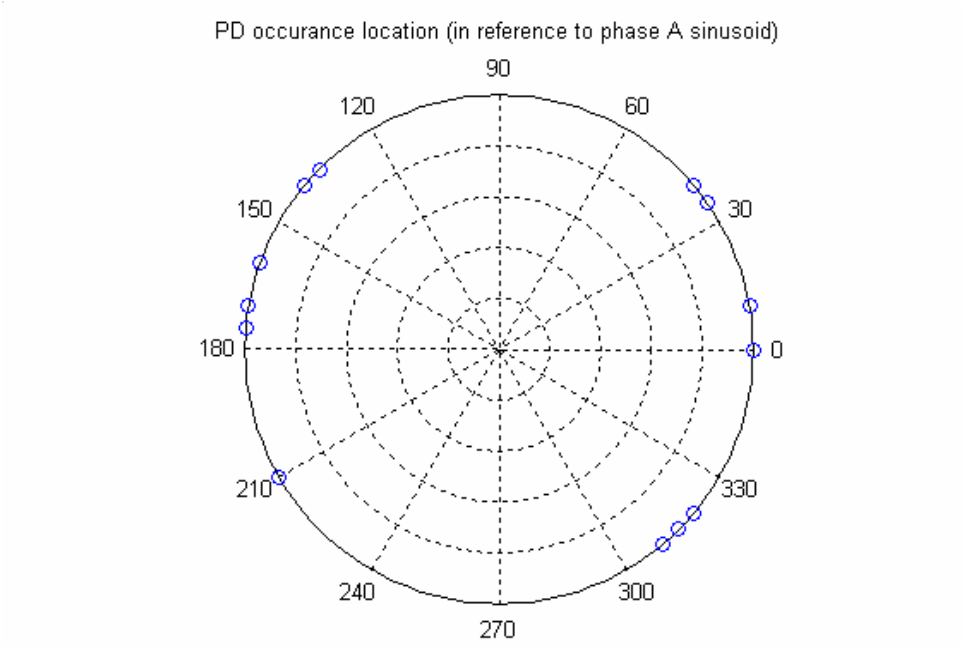

Fig 56. PD signal occurrence phases in reference to transformer voltage phase A sinusoid.

The phases where the PDs occur from the measurement can be represented in a polar plot form, shown in Fig 56. Note that, Table 4 data assumes there is no propagation time delay between the single PD source and the sensor. In reality, there is time delay

between the PD source and sensor. If we assume that the distance between a single PD source and the sensor is 4.2 meter, with the acoustic propagation velocity in oil about 1500 meter/second, we could calculate the time delay to be 0.0028 second, which corresponds to 50° in a 50Hz sinusoid cycle. 50Hz corresponds to the local electric frequency. The adjusted PD signal occurrence phases with time delay is shown in Fig 57.

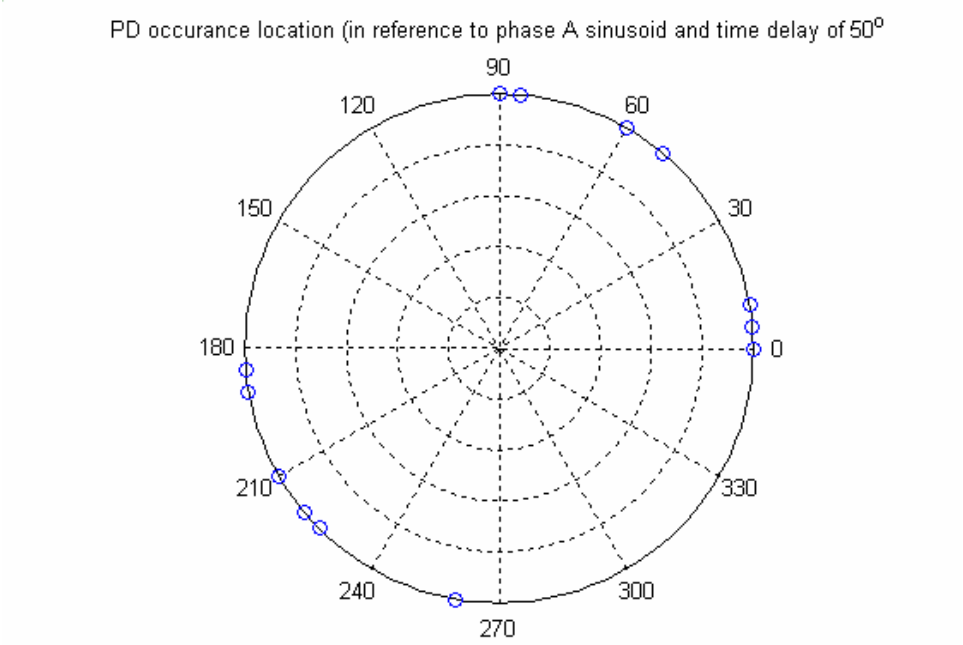

Fig 57. PD signal occurrence phases with assumed time delay (0.0028 second) between PD source and the fiber optic sensor in reference to transformer phase A voltage sinusoid.

If we relate the PD occurrence phases with assumed time delay between PD source and the sensor, we could obtain that the PD phases fall in the 1st and 3rd quadrant (0°-90° and 180°-270°, respectively).

Since this is a 3-phase transformer, we could shift the PD signal occurrence phases in reference to phase A by +120° or –120° to align with phase B (Fig 58) and phase C (Fig 60) voltage of the transformer. Again, we assume that the single PD source occurrence in phase B or phase C. If the single PD source were occurred in phase B, assuming the distance between the PD is 9.2 meters, the time delay would be 0.0061 second, which

corresponds to 110° in a 50Hz sinusoid cycle. Fig 59 shows the adjusted PD signal occurrence phases in reference to phase B sinusoid.

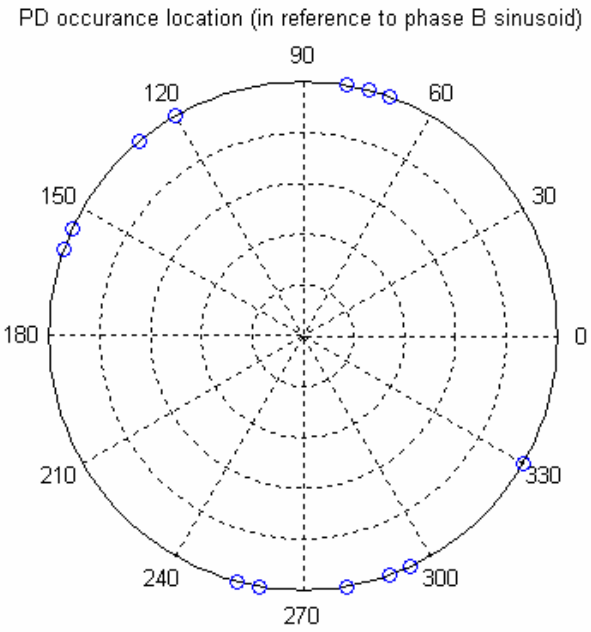

Fig 58. PD signal occurrence phases in reference to transformer voltage phase B voltage sinusoid

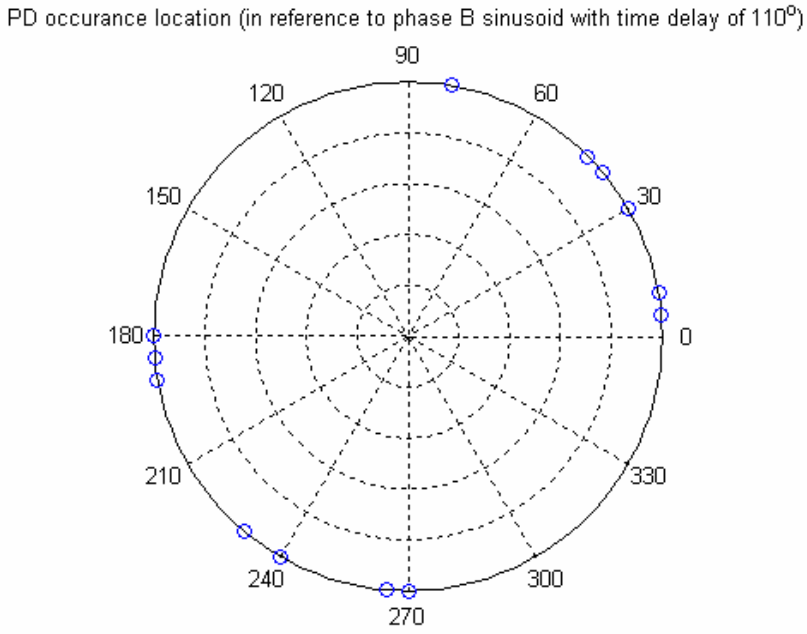

Fig 59. PD signal occurrence phases with assumed time delay (0.0061 second) between PD source and the fiber optic sensor in reference to transformer phase B voltage sinusoid

If the PD source was from phase C, shown in Fig 60, for the PD occurrence phases fall in the 1st and 3rd quadrant, the time delay between the source and sensor would have been 0.02 second, which corresponds to 350° delay in a 50Hz sinusoid cycle, shown in Fig 61. The distance between the source and sensor would be 30 meters and this distance is not realizable in the actual transformer geometry, so the PD would not be possible occurred at phase C.

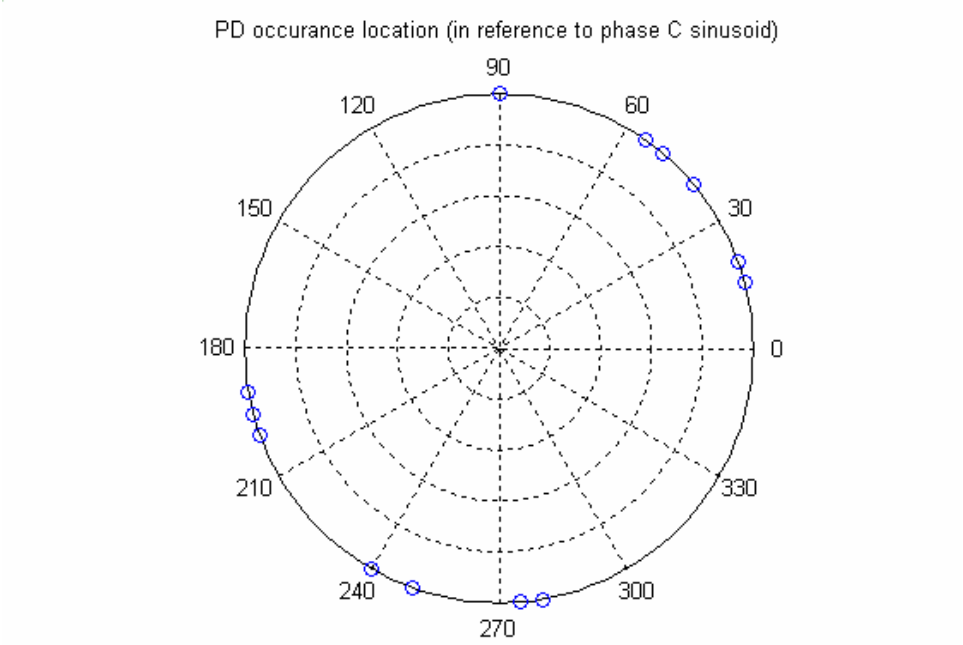

Fig 60. PD signal occurrence phases in reference to transformer phase C voltage sinusoid

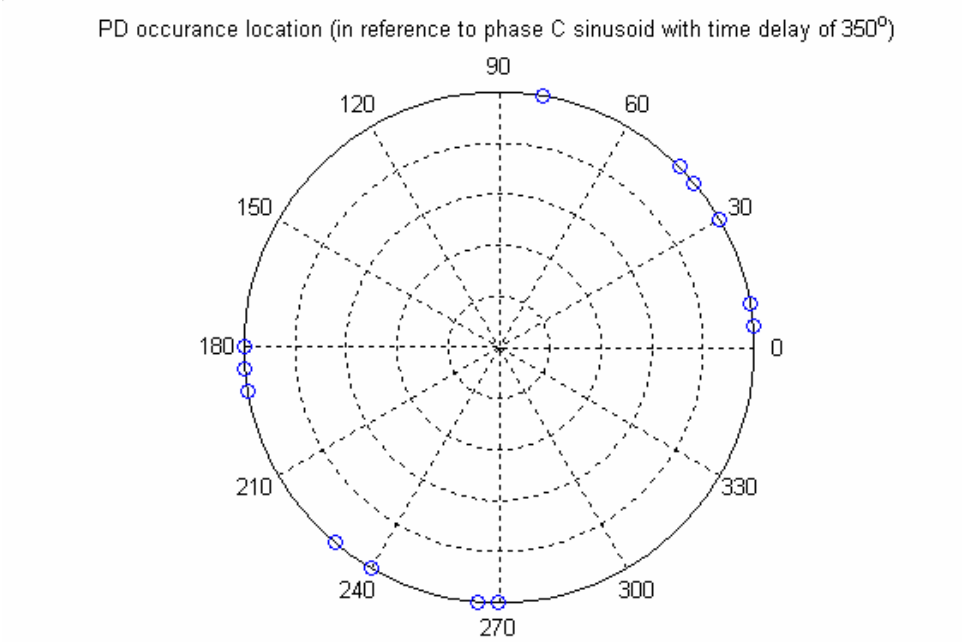

Fig 61. PD signal occurrence phases with assumed time delay (0.02 second) between PD source and the fiber optic sensor in reference to transformer phase C voltage sinusoid

More information on the measurement results by other teams who worked on the same project can be found in http://www.partialdischarge.co.uk/